

Chapter I

General Properties of Turbulent Jets

1.1. Fundamental Concepts

In many cases of motion of a liquid or gas, so-called tangential separation surfaces arise; the flow of fluid on either side of this surface is termed a jet. The jets may be moving in the same direction or in opposite directions. Tangential separation is experienced by such parameters as flow velocity, temperature, and specie concentration, though the distribution of static pressure proves continuous.

As is well known [4], the instability of the tangential separation surface causes eddies on it, which move in disorderly fashion both along and across the stream; this brings about an exchange of matter between neighboring jets; i.e., there is a transverse transfer of momentum, heat, and constituents. As a result, a region of finite thickness with a continuous distribution of velocity, temperature, and specie concentration is formed on the boundary between the two jets; this region is termed the turbulent jet boundary layer. At very low Reynolds numbers, this boundary layer may be laminar, but we shall not deal here with these comparatively rare cases.

The simplest case of a jet boundary layer is found during the discharge of fluid with a uniform initial velocity field ($u_0 = \text{const}$) into a medium moving at constant velocity ($u_\infty = \text{const}$), since here the thickness of the boundary layer in the initial section of the jet is equal to zero. The thickening of the jet boundary layer, which consists of particles of the surrounding medium carried along with it and particles of the jet itself that have been slowed down, leads, on the one hand, to an increase in the cross section of the jet and, on the other, to a gradual "eating up" of its nonviscous core — the region between the inside boundaries of the boundary layers. Figure 1.1 shows a simplified diagram of the jet.

The part of the jet in which there is a core of potential flow is termed the initial region (see Fig. 1.1).

As shown by numerous experiments, one of the fundamental properties of a jet of this kind is the fact that the static pressure is constant throughout the flow,* as a result of which the velocity

*In certain cases (when the jet interacts with an obstacle), the pressure may not remain constant, but we shall deal with these particular cases separately.

in the potential core of the jet remains constant. The "eating up" of the jet beyond the initial area shows up both in its widening as well as in variation of the velocity along its axis.

At a certain distance from the end of the initial area, the jet becomes similar in appearance to a flow of fluid from a source of infinitely small thickness (in an axially symmetric case the source is a point, and in a plane-parallel case it is a straight line perpendicular to the plane of flow of the jet).

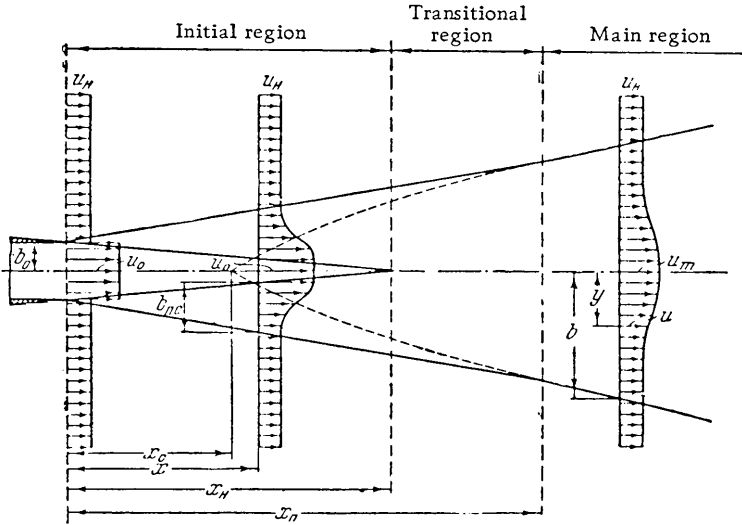


Fig. 1.1. Diagram of jet.

Use is often made of a simplified diagram of the jet in which it is assumed that the length of the transitional region is equal to zero; in this case the cross section in which the main and initial areas come together is termed the transitional cross section of the jet. If the transitional area is taken into account in the calculations, then the transitional cross section is considered to coincide with the beginning of the main area.

1.2. Submerged Jet

The type of turbulent jet most studied is one spreading through a medium at rest; a jet of this kind is said to be submerged. If the velocity field at the initial cross section of the submerged jet is uniform, the boundaries of the mixing layers form diverging surfaces, which intersect at the edge of the nozzle (in Fig. 1.2 at the initial cross section of the jet). On the outside, the boundary layer comes into contact with the stationary liquid, and the outside boundary is taken to mean that surface on all points of which the velocity component with respect to the x -axis is equal to zero ($u_x=0$). On the inside, the boundary layer changes to a constant

velocity core; hence, on the inner boundary of the boundary layer, the flow velocity is equal to the discharge velocity ($u_1 = u_0$).

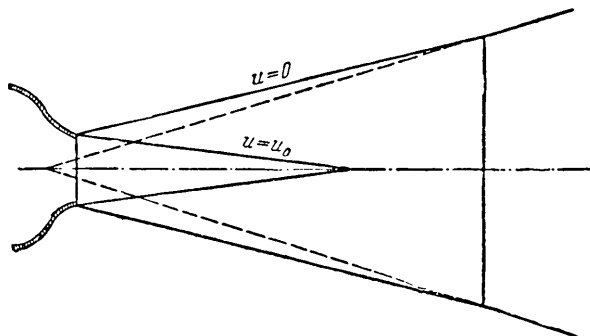


Fig. 1.2. Diagram of submerged jet.

In this description of the jet, it is assumed that the boundary layer is of finite thickness; in certain theories of the submerged jet, it is assumed that the boundary layer is of infinite thickness and has asymptotic profiles of velocity, temperature, and other quantities. Both these interpretations of the boundary layer can be reconciled in practice, since the asymptotic layer can be approximately replaced by a layer of finite thickness*.

1.3. Velocity Profiles in a Submerged Jet

A characteristic feature of a turbulent jet, as shown by theory and also by numerous experiments, is the smallness of the transverse velocity components in any section of the jet compared with the longitudinal velocity. Hence, if the x -axis is aligned with the axis of symmetry of the stream, the velocity components along the y -axis prove so small that they can be disregarded in engineering problems involving jet theory. Figure 1.3 shows curves for the velocity distribution (or to be more exact, the velocity components along the x -axis) at different cross sections of the principal area of a round air jet discharged into stationary air (Trüpel's experiments) [5]. The initial velocity of the jet $u_0 = 87$ m/sec. The radius of the initial section is $r_0 = 0.45$ m. The velocity profiles were determined at the following distances from the nozzle: $x = 0.6, 0.8, 1.0, 1.2,$ and 1.6 m.

As in studies made by other investigators, Trüpel's experiments show a continuous broadening of the velocity profile of the

*In this case the "boundaries" of the asymptotic layer are the surfaces on which the velocities (or, for example, the temperatures) differ from their limiting values by a small prescribed amount, for example 1%.

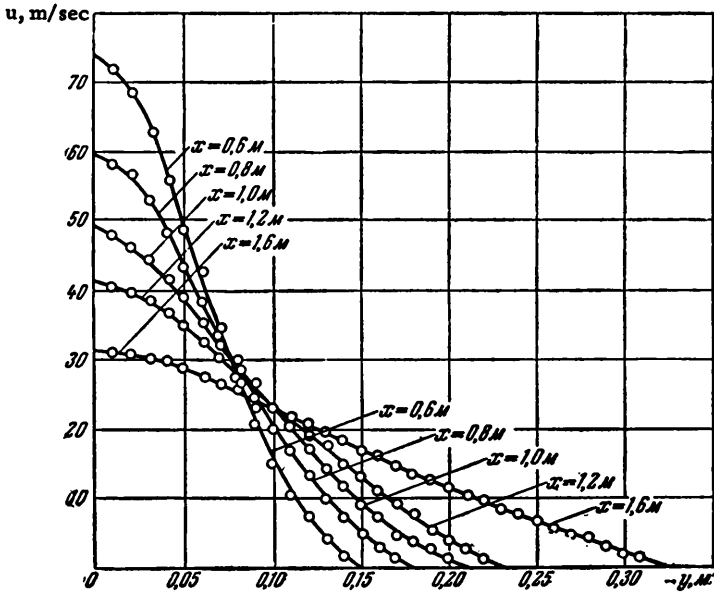


Fig. 1.3. Velocity profiles in different sections of an axially symmetric submerged jet from Trüpel's experimental data [5].

jet. The velocity profile becomes "lower" and "wider" with increasing distance from the beginning of the jet. This conclusion is reached when velocity profiles are plotted in physical coordinates (u, y). More interesting results are obtained when the same profiles are plotted in dimensionless form.

For example, instead of the absolute velocity, let us try to plot the ratio of the local velocity to the velocity on the jet axis u/u_m , and instead of the distance from the jet axis, let us plot the ratio of this distance to the distance between the axis and the point at which the velocity is equal to half the axial velocity y/y_c . The diagram obtained (Fig. 1.4) shows the similarity of the velocity profiles in all sections of the principal area of a round jet. Thus, at corresponding points on any two cross sections of the main part of the jet, the nondimensional velocities are the same. Obviously, we need not take y_c as the characteristic line, but could substitute, for example, the half-thickness of the jet b . The equality of the dimensionless velocities for corresponding points in the jet ($y_1/b_1 = y_2/b_2$) is then expressed in the following way

$$\frac{u_1}{u_{1m}} = \frac{u_2}{u_{2m}},$$

where u_1 and u_2 are the velocities at corresponding points of two cross sections of the jet; u_{1m} and u_{2m} are the appropriate velocities at the centers of these cross sections.

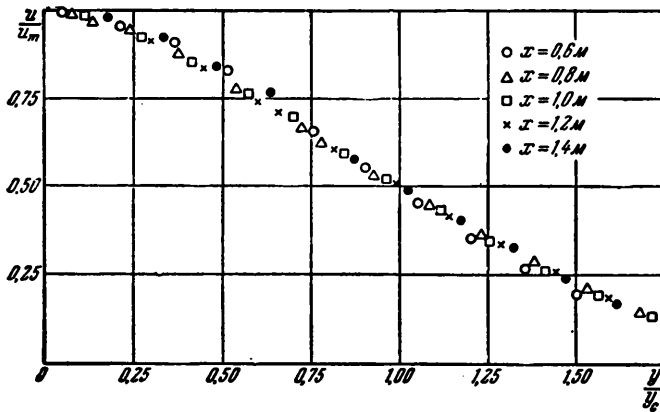


Fig. 1.4. Dimensionless velocity profile in axially symmetric submerged jet from Trüpel's experimental data [5].

The conclusions are valid for other types of jet besides round ones. They apply equally to plane-parallel jets discharged from a long slot. In order to see that this is so, we need only take a look at Förthmann's results [6]. He has studied the velocity profiles of an air jet emerging from a rectangular nozzle 0.03 m high and 0.65 m wide. The jet velocity at the outlet from the slot was 35 m/sec. Figure 1.5 plots the velocity profiles for jet sections at the following distances from the nozzle: $x=0, 0.2, 0.35, 0.5, 0.625,$ and 0.75 m. When they are replotted in dimensionless coordinates (the same ones as for Trüpel's experiments), the velocity profiles of the principal area of the plane jet, just as in the case of a round jet, are similar (Fig. 1.6).

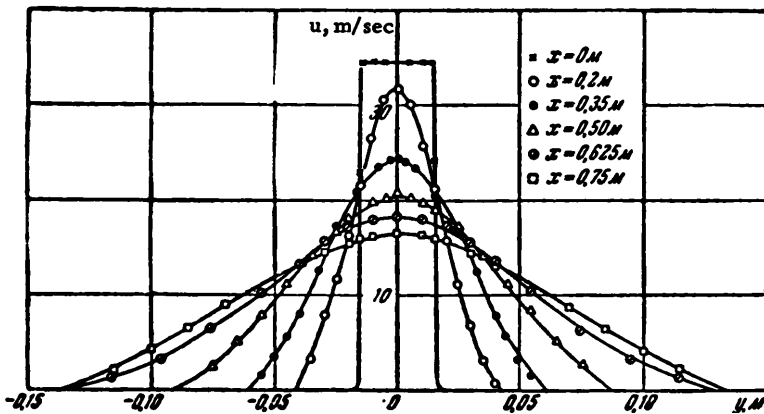


Fig. 1.5. Velocity profiles at different sections of a plane jet from Förthmann's experimental data [6].

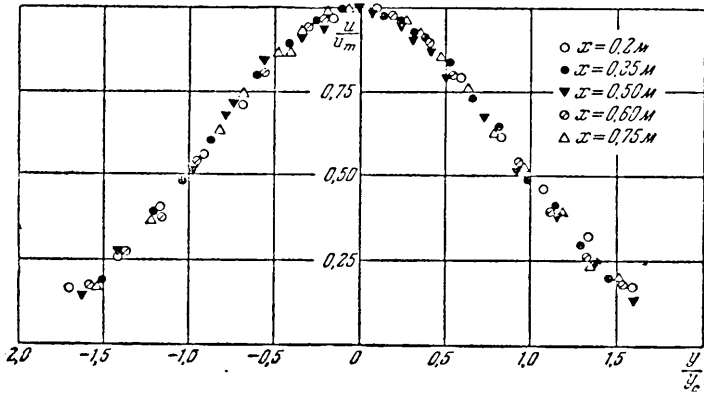


Fig. 1.6. Dimensionless velocity profile in plane jet according to Förthmann's experimental data [6].

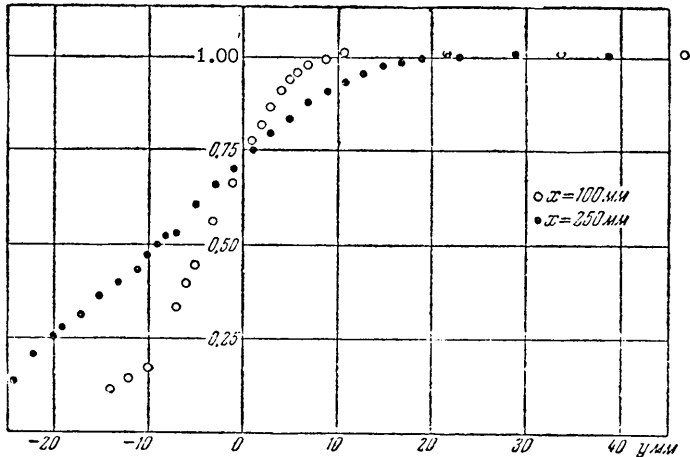


Fig. 1.7. Velocity profiles in different sections of boundary layer of axially symmetric jet from Abramovich's experimental data [3].

In 1938 the author made an experimental study of the initial region of an axially symmetric air jet discharged from a nozzle 100 mm in diameter at velocities up to 40 m/sec [3]. The velocity profiles obtained for the boundary layer of the initial area at distances from the nozzle $x=0.1$ and 0.25 m are plotted in Figure 1.7. The profiles shown in Figure 1.7 are plotted in Figure 1.8 in the dimensionless form

$$\frac{u}{u_0} = f\left(\frac{\Delta y_c}{\Delta y_b}\right),$$

in which u_0 is the velocity in the core of the unperturbed stream (discharge velocity); $\Delta y_c = y - y_c$ is the distance between the point of

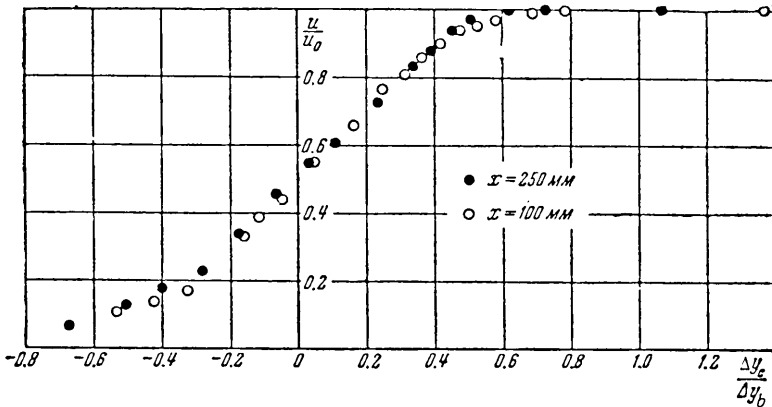


Fig. 1.8. Dimensionless velocity profile in the boundary layer of initial region of submerged axially symmetric jet ($r_0=50$ mm) according to Abramovich's experimental data [3].

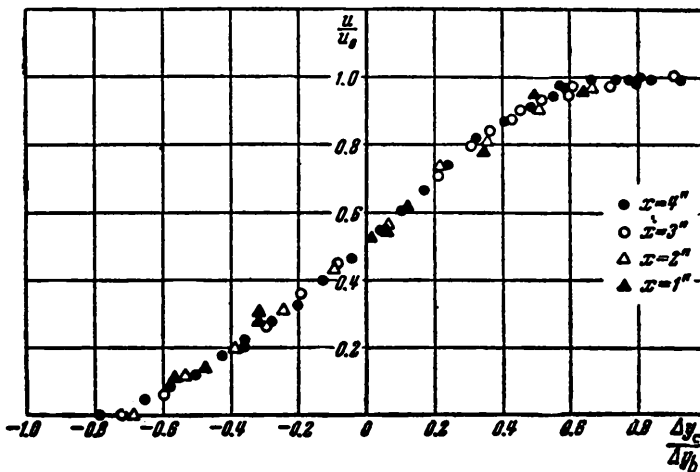


Fig. 1.9. Dimensionless velocity profile in boundary layer of initial region of plane jet ($b_0=12.7$ mm), from the experimental data of Albertson et al. [7].

measurement and the point at which the velocity is half what it is in the core ($u_c=0.5u_0$); $\Delta y_b = (y_{0.9} - y_{0.1})$ is the distance between the points at which the velocity is, respectively, 0.9 and 0.1 of the unperturbed stream velocity ($u/u_0=0.9$ and $u/u_0=0.1$); we shall consider this dimension to be the scale describing the thickness of the jet boundary layer; the exact determination of it on the basis of experiments is extremely difficult.

The results shown in Figure 1.8 indicate that in the initial area at small distances from the nozzle ($\frac{x}{d} < 3$) the boundary layer

velocity profiles at different cross sections of an axially symmetric jet are similar.

Figure 1.9 shows dimensionless velocity profiles obtained by Albertson, Dai, Jensen, and Rouse [7] in the boundary layer of the initial area of a plane-parallel air jet issuing into stationary air from a slot-shaped nozzle 1 inch high ($2b_0 = 25.4$ mm), at different distances from the nozzle exit ($\frac{x}{b_0} = 2, 4, 6, \text{ and } 8$). As we can see, here, too, the different velocity profiles lie along the same universal curve.

1.4. Spread of a Turbulent Submerged Jet

In a turbulent jet the components of velocity at any point can be decomposed into a time-averaged value plus a randomly varying perturbation

$$u = \bar{u} + u', \quad v = \bar{v} + v'$$

When averaged over some finite time interval, the fluctuation or pulsation components are equal to zero:

$$\bar{u}' = \bar{v}' = 0.$$

If the mean free path of a fluid particle (mixing length) in a turbulent stream is equal to l , when moved in a transverse direction, the particle reaches a layer in which the mean velocity differs from what it was in the layer from which the particle separated by the following value:

$$\Delta \bar{u} = l \frac{\partial \bar{u}}{\partial y}.$$

The loss in individuality of the fluid particle — its merging with the mass of the new layer — should be accompanied by a discontinuous variation (perturbation) in velocity of

$$u' = \Delta \bar{u}.$$

In other words, perturbations of the streamwise velocity component are of the order

$$u' \sim l \frac{\partial \bar{u}}{\partial y}.$$

It is usually assumed that the transverse perturbations in velocity v' are proportional to the streamwise perturbations u' , but have the opposite sign

$$-v' \sim u', \text{ i.e., } -v' \sim l \frac{\partial \bar{u}}{\partial y}.$$

The absence in the free stream of solid boundaries that might damp the oscillations of the particles led Prandtl [8] to assume that in this case the mixing length at any cross section of the stream was constant:

$$l(y) = \text{const.}$$

The variation in the mixing length along the x -axis $l=l(x)$ may be established by means of available experimental data. A sufficient basis for Prandtl's assumption is provided by the similarity of boundary layers in different cross sections of a free stream. As was mentioned earlier, this similarity has been established by a large number of experiments in which the velocity profiles prove universal when plotted in dimensionless coordinates

$$\frac{u}{u_m} = f\left(\frac{y}{b}\right), \quad (1.1)$$

i.e., they coincide for different sections of the jet. The similarity of boundary layers in the sections of the given free stream implies, among other things, the similarity of geometric dimensions. In other words, equality may be expected between the dimensionless mixing lengths for different sections of the stream

$$\frac{l_1}{b_1} = \frac{l_2}{b_2} = \dots = \text{const.} \quad (1.2)$$

Thus, it is sufficient to establish a law for the growth of the jet as a function of distance along the x -axis in order to define the way in which the mixing length increases. Prandtl [9] assumes that the growth of the jet (i.e., the rate at which the thickness of the jet boundary layer increases) is controlled by the transverse perturbation velocity

$$\frac{db}{dt} \sim v' \sim -l \frac{\partial \bar{u}}{\partial y}. \quad (1.3)$$

Because of the similarity of velocity profiles in different cross sections of the jet, it is possible to write

$$\frac{\partial \bar{u}}{\partial y} \sim \frac{u_m}{b} \quad (1.4)$$

and, hence, according to Eqs. 1.2, 1.3, and 1.4,

$$\frac{db}{dt} \sim \frac{l}{b} u_m \sim u_m. \quad (1.5)$$

On the other, hand, rate of growth of the jet

$$\frac{db}{dt} = \frac{db}{dx} \frac{dx}{dt} \sim \frac{db}{dx} u_m. \quad (1.6)$$

A comparison of Eqs. 1.5 and 1.6 provides a solution of the problem of establishing the law governing the increase in thickness of the submerged jet and the mixing length in the direction of flow

$$\frac{db}{dx} = \text{const}, \quad b = x \cdot \text{const}, \quad l = cx. \quad (1.7)$$

The derived linear law for the increase in the jet thickness and mixing length along the stream holds for jets of different shape: the boundary layer of an infinite plane stream, the plane-parallel jet, and the axially symmetric jet. In all three cases the law applies when the velocity profiles in the submerged jet are universal.

1.5. Lines of Constant Velocity in a Submerged Jet

Let a uniform, semi-infinite, plane-parallel jet issue from the wall AO at a velocity u_0 , and starting from point O merge with the surrounding motionless fluid.* The previously established linear increase in thickness of the boundary layer in conjunction with the universal or self-similar nature of the velocity profile means that along any ray $O\varphi$ drawn from the origin of the coordinates (which coincides with point O at which the thickness of the boundary layer is zero), the velocity remains constant.

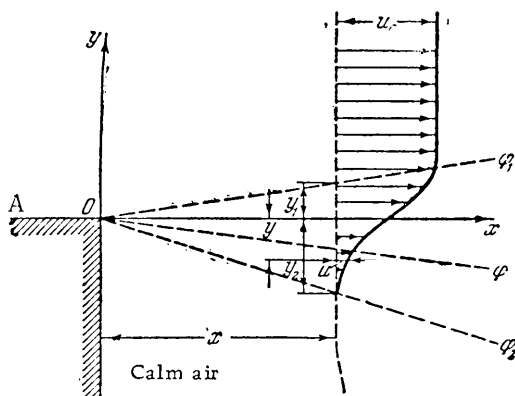


Fig. 1.10. Diagram of boundary layer in submerged jet.

Indeed, the similarity of the velocity profiles implies the equality of velocities at corresponding points in the stream; i.e., at

$$\frac{y_1}{b_1} = \frac{y_2}{b_2} = \frac{y_3}{b_3} = \dots = \text{const}$$

*If the plane Oxy in Fig. 1.10 is horizontal, it is not necessary to consider gravity, which has an effect, for example, on a non-isothermal gas jet.

there results

$$\frac{u_1}{u_0} = \frac{u_2}{u_0} = \frac{u_3}{u_0} = \dots = \text{const.}$$

But according to Eq. (1.7)

$$b = x \cdot \text{const};$$

from which we find that on the ray

$$\frac{y}{x} = \text{const} \quad (1.8)$$

the following condition is satisfied

$$\frac{u}{u_0} = \text{const.} \quad (1.9)$$

Thus, in a turbulent boundary layer of a plane-parallel submerged stream, the rays converging at the point where the thickness of the layer is zero constitute equal-velocity lines. This result refers both to plane-parallel flow and the boundary layer in the initial area of a round jet, since experiments show that in this case, too, the velocity fields are universal.

The origin of the coordinates for the equal-velocity lines in the boundary layer in the initial area of the jet is the outlet edge of the nozzle (when the velocity field in the initial section of the jet is uniform).

It should be pointed out that in the initial area, equal-velocity lines plotted for physical (u) and dimensionless (u/u_0) velocities coincide, since the velocity u_0 along the length does not vary in the core of the flow.

The shape of these lines in the main sector of a submerged jet depends on the method used to determine the dimensionless velocity. If the dimensionless velocity is obtained by dividing the local velocity by the discharge velocity from the nozzle (u/u_0), just as for the physical velocity, the lines of the principal area form a fan, shown in Figure 1.11. For the dimensionless velocity, calculated by dividing the local velocity by the axial velocity in the corresponding cross section (u/u_m), the lines are straight and converge at the pole of the jet (Fig. 1.12). This result stems from the fact that the dimensionless velocity is a function of only the relative position of the point in the cross section of the jet

$$\frac{u}{u_m} = f\left(\frac{y}{b}\right). \quad (1.10)$$

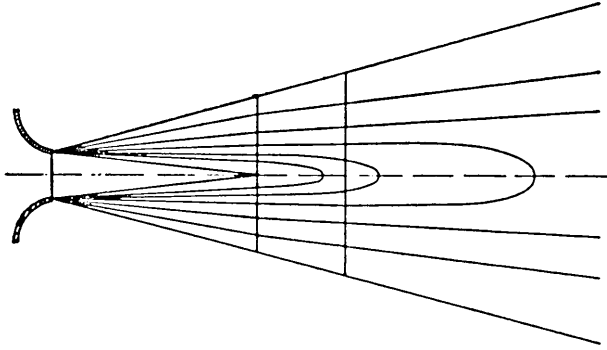


Fig. 1.11. Equal velocity lines in submerged jet.

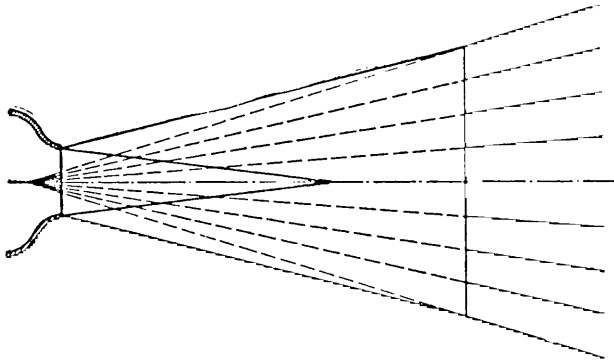


Fig. 1.12. Equal velocity lines ($u/u_m = \text{const}$) in main region of submerged jet.

On account of the linearity of the thickening of the jet (Eq. 1.7), Eq. 1.10 may be brought to the form:

$$\frac{u}{u_m} = f\left(\frac{y}{x}\right),$$

which indeed proves that the equal velocity lines for the dimensionless velocity u/u_m are rays which intersect at the pole of the jet. The rectilinearity of these lines for a dimensionless velocity (u/u_m) is found both in axially symmetric and plane-parallel cases. The experimental data given below are clear proof of this.

Figure 1.13 plots five lines on each of which the dimensionless velocity is constant: $u/u_m = 0.9, 0.7, 0.5, 0.3,$ and 0.1 . The experimental points are taken from the Förthmann experiments mentioned earlier for a plane-parallel submerged jet, discharged from a slot of height $2b_0 = 30$ mm and width 650 mm, and from Trüpel's experiments for a submerged round jet with an initial diameter $2r_0 = 90$ mm.

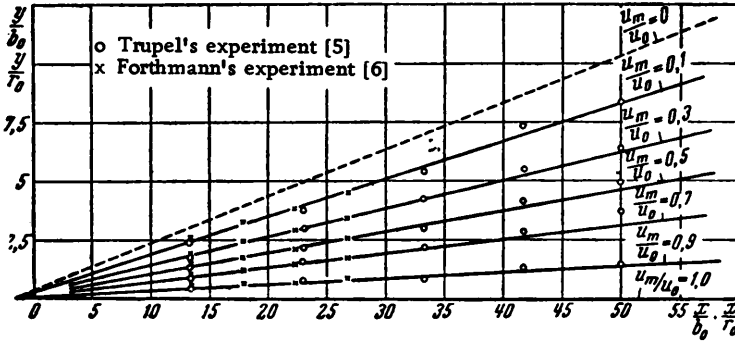


Fig. 1.13. Equal dimensionless velocity lines in submerged jet.

As can be seen, Förthmann's experimental points (crosses) and Trüpel's points (rings) lie close along the same ray for each dimensionless velocity ($u/u_m = \text{const}$), and the rays for the five velocities converge at the same point.

The angular coefficient of the ray $u_c = 0.5u_m$, which is roughly the same for plane-parallel and axially symmetric submerged jets, is approximately equal to

$$\frac{v_c}{x} = 0.097. \tag{1.11}$$

1.6. Velocity Variation Along the Axis of a Submerged Jet

As shown by experiment, the pressure in the jet is virtually invariable and equal to the pressure in the surrounding space. On account of this the total momentum of air mass per second should be the same in all the cross sections of the jet:

$$\int_0^m u \, dm = \int_0^F \rho u^2 \, dF = \text{const}, \tag{1.12}$$

in which dm is the mass flowing through an element of the cross section of the jet per unit time; ρ is the air density; dF is the area of the element.

For a round jet the condition for constant total momentum can be written in the following way:

$$u_m^2 x^2 \int_0^r \left(\frac{u}{u_m}\right)^2 \frac{y}{x} \frac{dy}{x} = \text{const}, \tag{1.13}$$

in which u_m is the velocity in the center of the given sections, x is the distance between the given section and the jet pole, y is the

radius, and r is the radius of the outer boundary of the jet section in question.

On account of the universal nature of the velocity profiles, the dimensionless velocity (u/u_m) at the selected point is a function of only the dimensionless coordinate (y/x) of a ray drawn from the pole through this point,

$$\frac{u}{u_m} = f\left(\frac{y}{x}\right).$$

Hence,

$$\int_0^{\frac{r}{x}} \left(\frac{u}{u_m}\right)^2 \frac{y}{x} \frac{dy}{x} = \text{const.}$$

We find as a result of the Eq. 1.13 that the velocity in the center of the section of an axially symmetric submerged jet is inversely proportional to the distance from the pole

$$u_m = \frac{\text{const}}{x}. \quad (1.14)$$

For a plane-parallel submerged jet, the fact that the momentum is constant gives us the relationship

$$u_m^2 x \int_0^{\frac{b}{x}} \left(\frac{u}{u_m}\right)^2 \frac{dy}{x} = \text{const}, \quad (1.15)$$

in which b is the semithickness of the section. On account of the universal nature of the velocity profiles,

$$\int_0^{\frac{b}{x}} \left(\frac{u}{u_m}\right)^2 \frac{dy}{x} = \text{const.}$$

Hence the drop in velocity along the axis of a plane-parallel jet takes the following form:

$$u_m = \frac{\text{const}}{\sqrt{x}}. \quad (1.16)$$

The proportionality constants in Eqs. 1.14 and 1.16 are determined by the integrals of Eqs. 1.13 and 1.15, and in order to calculate the latter, we must know the velocity distribution in the

cross sections of the jet. Because of the universal nature of the velocity profiles, all we need do is determine the velocity distribution experimentally in only one section in the main region of the jet. The theory described below enables us to solve this problem theoretically.

A shortcoming of Eqs. 1.14 and 1.16 is the fact that the distance x is reckoned from the pole of the jet and not from its initial section. In Section 9 we derive more suitable relationships, in which the distances are taken from the beginning of the jet. Equations 1.14 and 1.16, as will be shown later, agree well with experimental data.

1.7. Heat Transfer in a Submerged Jet

In engineering we often encounter a submerged jet in which the temperature differs from that of the surrounding medium.

The solution of the problem of heat transfer from air at rest to a jet (and back again) is possible only if the variations in temperature along the jet and in its cross sections are known.

Let us introduce consideration of the temperature changes:

a. the difference between the temperature at a given point in the jet and in the surrounding medium (room)

$$\Delta T = T - T_{\text{H}};$$

b. the difference between the temperature on the jet axis and in the surrounding space

$$\Delta T_m = T_m - T_{\text{H}};$$

c. the difference between the temperature in the initial cross section of the jet (at the mouth of the nozzle) and the surrounding space

$$\Delta T_0 = T_0 - T_{\text{H}}.$$

The nature of the distribution of the magnitudes of the temperature differences in a submerged jet, as shown by experiment, is similar to that of the velocity distribution. In the constant velocity core of the initial region the temperature is constant and equal to the temperature of the fluid in the initial cross section of the jet. In the main region the temperature boundaries of the jet expand with distance from the nozzle since the temperature difference on the flow axis decreases.

Figure 1.14 shows the dimensionless temperature field found by the author [3] for a boundary layer in the initial region of an air jet of round section, 100 mm in diameter, at a distance of 250 mm from the nozzle (white dots); the abscissa is the same as in Figures 1.8 and 1.9. For the purpose of comparison, the velocity field obtained for the same jet section (black dots) has been transferred

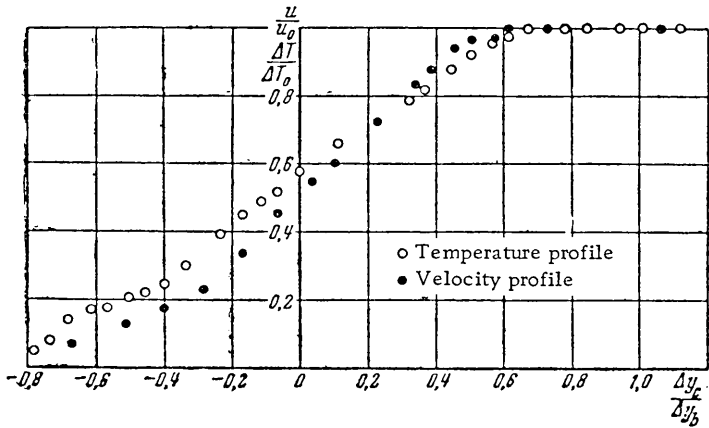


Fig. 1.14. Dimensionless temperature difference profile in boundary layer of axially symmetric jet according to Abramovich's data [3].

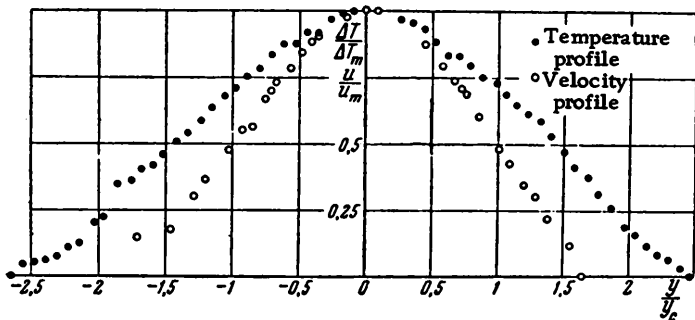


Fig. 1.15. Dimensionless temperature and velocity profiles in main region of plane jet according to Reichardt's experimental data [10].

to Figure 1.14 from Figure 1.8. In this experiment the discharge velocity of the jet from the nozzle amounted to $u_0 = 25$ m/sec, and the temperature difference at the nozzle outlet section was $\Delta T_0 = 35^\circ\text{C}$.

The graph in Figure 1.15 plots the dimensionless temperatures in the main region of a plane jet as

$$\frac{\Delta T}{\Delta T_m} = f\left(\frac{y}{y_c}\right),$$

in which y is the variable distance between the point and the axis (ordinate); y_c is the ordinate of the point (at the same section) at which the velocity is half what it is on the jet axis.

The experimental data have been taken from Reichardt [10], who investigated a submerged air jet discharged from a long,

rectilinear slot with sharp edges and 7×150 mm in size; the discharge velocity was about 50 m/sec and the initial temperature difference 10 to 20°C . For purposes of comparison, Figure 1.15 also shows the dimensionless velocity field for the same jet. The velocities and temperatures were measured by Reichardt at 400 mm from the slot; the temperature fields were found to be considerably fuller than the velocity fields.

Figure 1.16 plots the dimensionless temperature difference $\Delta T / \Delta T_m = f(y/y_c)$; the data were obtained by Stark [11] for different cross sections of the main region of an axially symmetric air jet discharged into stationary air. In his experiments, Stark used a nozzle with diameter $2r_0 = 41.5$ mm, discharge velocity $u_0 = 20$ m/sec and initial temperature difference $\Delta T_0 = 15^\circ\text{C}$. All the points lie roughly along a universal curve, although they relate to different cross sections at distances from the nozzle ranging from 10 to 70 nozzle radii.

For purposes of comparison, Figure 1.15 shows the velocity fields for the same sections. Similar results were obtained by Ruden [12] in his experiments. Figures 1.14 to 1.16 show that the experimental curves for the dimensionless velocity and dimensionless temperature obtained for the same cross section of a submerg-ed jet do not coincide.

The theoretical laws governing the distribution of temperature in the cross sections of the jet are given in Chapter 2.

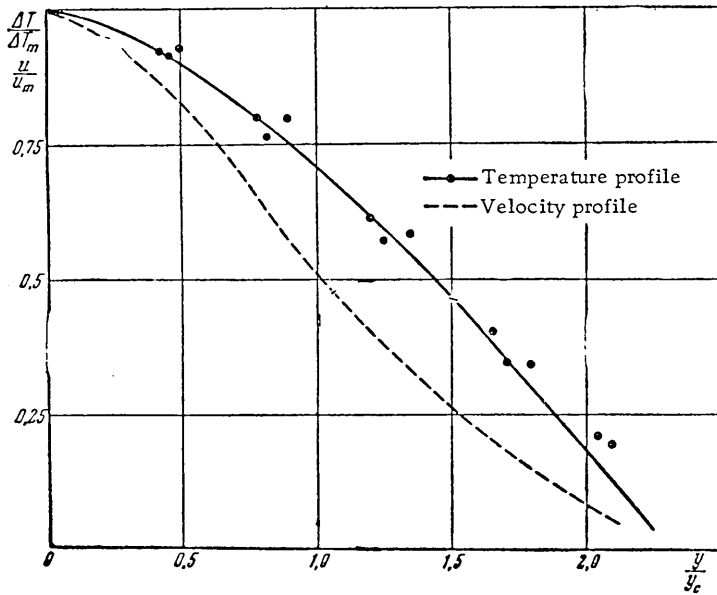


Fig. 1.16. Dimensionless temperature differences and velocity profiles in main region of axially symmetric jet according to Stark's data [11].

The distribution of temperature along the axis of the main region of the jet can be established in the same way as for the velocities, except that instead of the constant value of the momentum, the constant heat content of the jet must be used. Indeed, in the determination of the heat content of the jet from the temperature difference, the fluid sucked up by the jet from the surrounding space does not contribute to the heat transfer, since the temperature difference is equal to zero ($\Delta T_{\text{u}} = 0$). In other words, the surplus heat content of the entire mass of fluid passing through a jet section chosen at random is equal to the surplus heat content of the initial mass emerging over the same interval of time from the nozzle.

The diffusion of heat through a jet shows up in its transfer across the boundary between the initial mass and the incorporated mass, on account of which, as pointed out earlier, the temperature on the jet axis drops, while the temperature field in the cross sections is gradually "smoothed" out. The constancy of the heat content of the free jet, calculated in terms of the temperature difference, is expressed by the following relationship (see Eq. 1.12).

$$\int_0^m \Delta T dm = \int_0^F \rho u \Delta T dF = \text{const}; \quad (1.17)$$

for a jet of circular section,

$$x^2 u_m \Delta T_m \int_0^{\frac{r}{x}} \frac{\Delta T}{\Delta T_m} \frac{u}{u_m} \frac{y}{x} \frac{dy}{x} = \text{const}. \quad (1.18)$$

Because of the similarity of the profiles in different cross sections of the jet, the dimensionless isotherms, just as the equal-velocity lines, are rectilinear rays intersecting at the pole of the jet

$$\frac{\Delta T}{\Delta T_m} = 0 \left(\frac{y}{x} \right), \quad (1.19)$$

in which x is the distance between the pole and the section under discussion; y is the distance between the selected point and the center of the section where the temperature rise is ΔT_m .

Equation 1.19 implies that the integral in Eq. 1.18 is a constant. Hence, consideration of Eq. 1.14, gives the law of the drop in the temperature along the axis of a circular jet:

$$\Delta T_m = \frac{\text{const}}{x}. \quad (1.20)$$

Further on, it will be shown that Eq. 1.20 agrees with experimental data.

Jet theory enables the calculation of the constant in Eq. 1.20, and its value is not equal to the constant in Eq. 1.14. This is because of the difference in the universal profiles of temperature and velocity in the submerged jet. The problem has been elaborated in greater detail in a special section on equations for temperature distribution along the jet axis and in its cross sections.

In a plane-parallel jet the conservation of the surplus heat content can be expressed in the following way:

$$\Delta T_m u_m x \int_0^{\frac{b}{x}} \frac{\Delta T}{\Delta T_m} \frac{u}{u_m} \frac{dy}{x} = \text{const.} \quad (1.21)$$

Since the integral in Eq. 1.21 is constant, by taking Eq. 1.16 into account, we can find the drop in temperature along the axis of a plane-parallel jet:

$$\Delta T_m = \frac{\text{const}}{\sqrt{x}}. \quad (1.22)$$

To round off the preliminary analysis of the transfer of heat in a submerged jet, let us prove the theorem of the relationship between the mean temperatures and mean velocities. The fact that momentum in the jet is constant implies that the product of the mass per second flowing through a random section of the jet and the mean velocity is a constant:

$$m u_{c2} = m_0 u_0, \quad \text{i.e.,} \quad \frac{m u_{c2}}{m_0 u_0} = 1. \quad (1.23)$$

Furthermore, the fact that the heat content is constant means that the product of the mass flow and the mean temperature difference does not change, either, from section to section:

$$m \Delta T_{c2} = m_0 \Delta T_0, \quad \text{i.e.,} \quad \frac{m \Delta T_{c2}}{m_0 \Delta T_0} = 1. \quad (1.24)$$

By comparing Eqs. 1.23 and 1.24 we find that the drop in the mean temperature along the free jet conforms to the same law as the drop in mean velocity:

$$\frac{\Delta T_{c2}}{\Delta T_0} = \frac{u_{c2}}{u_0}. \quad (1.25)$$

It is interesting to observe that Eq. 1.25 describing the relationship between the mean values still holds, despite the fact that the temperature and velocity profiles in the submerged jet are dissimilar.

To avoid errors in the use of Eq. 1.25, we will give the exact definition of the concepts "mean velocity" and "mean temperature."

Generally speaking, the mean velocity can be calculated in different ways; here the results obtained are not the same, but depend on the physical meaning attributed to the word "mean."

Most frequently the mean velocity is taken to be the mean arithmetic velocity, which is represented by the ratio of the flow of fluid per second to the cross-sectional area

$$u_{c1} = \frac{m}{\rho_c F} = \frac{\int_0^F \rho u dF}{\rho_c F} \quad (1.26)$$

The mean arithmetic velocity is obtained by averaging with respect to area. The mean velocity can also be obtained as a ratio of the momentum per second to the mass flow per second:

$$u_{c2} = \frac{l}{m} = \frac{\int_0^m u dm}{\int_0^F \rho u dF} = \frac{\int_0^F \rho u^2 dF}{\int_0^F \rho u dF} \quad (1.27)$$

The value found from Eq. 1.27 is termed the mean-square velocity. It is found by averaging with respect to the mass rate flow of fluid. Naturally, the values u_{c1} and u_{c2} need not be the same, and the difference between them increases as the nonuniformity of the velocity field increases. In the case of a submerged jet, as will be shown later on, the mean arithmetic and mean-square velocities differ very considerably. The field of application of each of these concepts will be shown separately. The mean temperature also depends on the averaging method.

In practical calculations the average temperature according to mass flow of the fluid is almost always applied; hence, from now on we shall take the mean temperature to be the ratio of the heat content of the mass of fluid per second to the mass per second:

$$\Delta T_{c2} = \frac{\int_0^m \Delta T dm}{m} = \frac{\int_0^F \Delta T \rho u dF}{\int_0^F \rho u dF} \quad (1.28)$$

Returning to Eq. 1.25, we should note that the equality of the dimensionless mean temperature difference and mean velocity is valid only for the mean-square velocity, i.e., for cases in which the latter is derived by averaging with respect to mass flow.

1.8. Diffusion of Constituents in a Submerged Jet

In appropriate sections of this book it is shown that the diffusion of any kind of substance which is sometimes found in a jet in the suspended state (for example, gas mixtures, drops of fuel or dust) has very much in common with the propagation of heat.

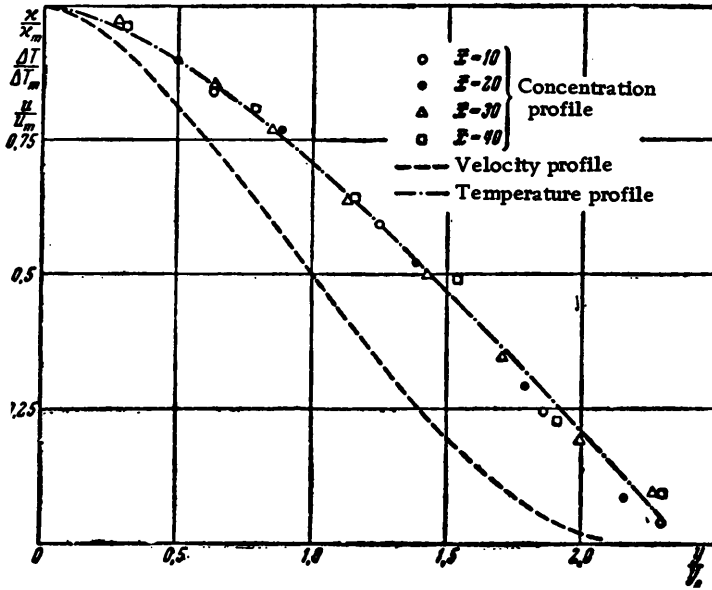


Fig. 1.17. Dimensionless profiles for temperature difference, concentration of admixture and velocity in main region of plane jet from data given by Abramovich and Borodachev ($\bar{x}=x/b_0$).

Figure 1.17 shows profiles for the dimensionless concentration by weight of carbon dioxide, obtained by the author in collaboration with V. Ya. Boradachev in an experimental investigation of the main region of a plane-parallel jet of carbon dioxide emerging into pure, stationary air:

$$\frac{x}{x_m} = f\left(\frac{y}{y_c}\right),$$

in which $x = G_{CO_2}/G_{803}$ is the concentration by weight, i.e., the ratio of the content of carbon dioxide by weight to the content of air by weight per unit volume at an arbitrary point in the cross section of the jet; x_m is the concentration by weight of CO_2 on the jet axis, y is the distance between the axis and the point of measurement; y_c is the distance between the axis and the point at which the velocity difference is half what it is on the axis. The nozzle from which the jet of gas was discharged had a rectangular outlet

section with sides $2b_0=3$ mm and $2h_0=30$ mm, i.e., with a side ratio 1:10. The concentration fields were measured in the plane of symmetry parallel to the smaller side of the rectangle at the following distances from the nozzle exit: $x/b_0=10, 20, 30,$ and 40 for a discharge velocity $u_0=55.9$ m/sec. The concentration of carbon was determined in two ways: by chemical analysis of a gas sample taken from the jet and by processing photographs taken with an interferometer. Both methods produced virtually the same results (the discrepancy was the same as the spread of points in the chemical method, which did not exceed 3% of the local concentration on the jet axis). As can be seen from Figure. 1.17, the dimensionless concentration fields of CO_2 obtained at various cross sections of the jet lie along a universal curve that does not coincide with the curve for the dimensionless velocity (broken line) obtained for the same cross sections; at the same time, the dimensionless temperature curve (dots and dashes), which we have transferred from Figure 1.16, passes very close to the concentration field profile.

In cases in which there is an admixture in the surrounding medium as well, it is advisable to introduce the concept of the "concentration difference" (Δx is the difference between the local concentration of the admixture in the jet and the concentration of the same admixture beyond the jet). Obviously, the surplus concentration of admixture is similar to the surplus heat content and is the same for different sections of the jet:

$$\int_0^m \Delta x \, dm = \int_0^F \rho \Delta x u \, dF = \text{const.}$$

The constancy of the surplus concentration of admixture as well as the similarity of the concentration fields in the cross section enables us to find the law governing the variation in concentration along the jet axis.

In the main region of an axially symmetric jet, under the condition of preservation of surplus constancy of concentration,

$$x^2 u_m \Delta x_m \int_0^{\frac{r}{x}} \frac{\Delta x}{\Delta x_m} \frac{u}{u_m} \frac{y}{x} \frac{dy}{x} = \text{const.} \quad (1.29)$$

Here Δx_m is the surplus concentration of admixture on the jet axis. In view of the universality of the velocity and concentration distributions in cross sections of the jet, the integral on the left-hand side of Eq. 1.29 has a constant value; hence if Eq. 1.16 is taken into account,

$$\Delta x_m = \frac{\text{const}}{x}, \quad (1.30)$$

that is, the surplus concentration of admixture along the axis of the main region of a submerged round jet is inversely proportional to the distance from the pole of the jet.

In the case of a plane jet, the constancy of the surplus of admixture concentration is expressed by the equality

$$u_m^2 x \int_0^{\frac{b}{x}} \frac{\Delta x}{\Delta x_m} \frac{u}{u_m} \frac{dy}{x} = \text{const.} \quad (1.31)$$

The integral contained on the left-hand side of Eq. 1.31, given universal distribution of velocity and surplus concentration, is a constant, hence the difference in concentration of the admixture along the axis of the main sector of a plane-parallel submerged jet varies in inverse proportion to the square root of the distance from the jet pole:

$$\Delta x_m = \frac{\text{const}}{\sqrt{x}}. \quad (1.32)$$

On the basis of the same condition of preservation of the constancy of the surplus of admixture, we find that the dimensionless concentration, averaged with respect to mass flow, is equal to the dimensionless velocity, averaged with respect to mass flow which, as was shown in the preceding paragraphs, is in turn equal to the dimensionless mean temperature difference:

$$\frac{\Delta x_{c2}}{\Delta x_0} = \frac{\Delta T_{c2}}{\Delta T_0} = \frac{u_{c2}}{u_0}, \quad (1.33)$$

in which Δx_{c2} is the difference between the concentration averaged over mass flow (x_{c2}) in a given cross section of the jet and the concentration of the same specie in the surrounding medium (x_0).

Further on it will be shown that the fields of the dimensionless surplus admixture and temperature difference coincide; this is because the mechanism of the transfer of heat and of admixtures in a turbulent stream is the same.

1.9. Velocity, Temperature, and Concentration Profiles in a Turbulent Jet Spreading into an External Stream of Fluid

Numerous experiments show that the profiles of velocity, temperature, and admixture concentration in a turbulent jet spreading through an external stream of fluid flowing in the same direction as the jet ("coflowing") are the same as in a submerged jet.

Figure 1.18 shows a universal velocity profile obtained by Forstall and Shapiro [14] in their experiments in the principal region of an axially symmetric jet of air discharged into an air

stream with the same direction and temperature; the dimensionless velocity differences are plotted against the dimensionless ordinates

$$\frac{u - u_n}{u_m - u_n} = f\left(\frac{y}{y_c}\right), \quad (1.34)$$

in which u_n is the velocity of the external stream; y_c is the distance between the axis of the stream and the point at which the velocity difference is half its maximum: $u_c - u_n = 0.5 (u_m - u_n)$. The experiments were carried out at discharge velocities up to 70 m/sec and a coflowing stream velocity of up to 28 m/sec at the following velocity ratios: $m = u_n/u_0 = 0.2, 0.25, \text{ and } 0.46$. The diameter of the nozzle discharging the active jet was 6.4 mm in one series of

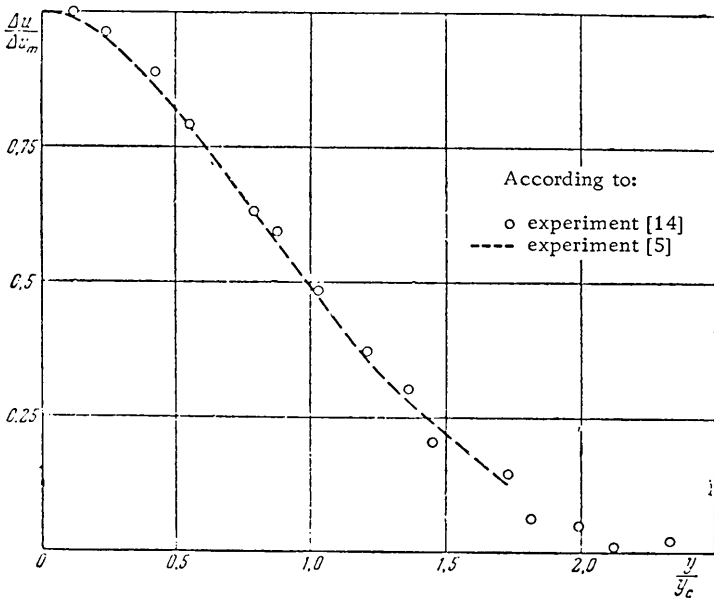


Fig. 1.18. Dimensionless velocity difference profile in main region of axially symmetric air jet spreading through coflowing stream of air from experimental data obtained by Forstall and Shapiro [14].

experiments and 25.4 mm in the second series; the diameter of the outer stream nozzle was 102 mm. The measurements were taken between the beginning of the principal region and the section 136 nozzle diameters from its exit. For purposes of comparison, Figure 1.18 shows the velocity profile of a submerged jet (broken line) taken from Trüpel's experiments (see Fig. 1.4); the universal velocity profiles both with and without a coflowing stream proved virtually identical.

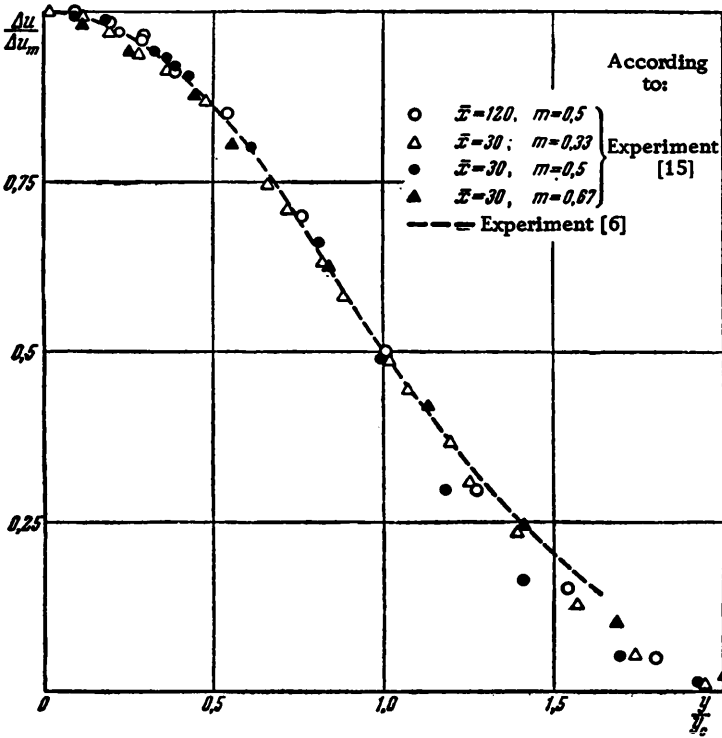


Fig. 1.19. Dimensionless surplus velocity profile in main sector of plane air jet spreading through co-flowing stream of air according to Weinstein's data [15] ($\bar{x}=x/r_0$).

Figure 1.19 shows, in the same coordinates as in Figure 1.18, the dimensionless surplus velocities (velocity differences) obtained by Weinstein, Osterle, and Forstall [15] with an experimental set-up which produced a plane air jet of thickness $2b_0=12.7$ mm into a plane air stream in the same direction of thickness $2b_0=278$ mm; the width of the initial cross sections of the jet and external stream were the same and amounted to 302 mm. The planes of symmetry of both streams coincided. The velocity of the jet ranged from 30 to 44 m/sec, and the velocity of the external stream from 15 to 22 m/sec; the experiments produced the following velocity ratios for the two streams: $m=u_1/u_0=0.33, 0.5,$ and 0.67 . The points shown in Figure 1.19 are for cross sections at distances of $x/b_0=30$ and 120 from the initial section.

For purpose of comparison, Figure 1.19 shows the velocity profile obtained by Förthmann (broken line) for a plane submerged jet; transferred from Figure 1.6. As we can see, the distribution of surplus velocity in a plane jet with a coflowing stream can be expressed by the same universal relationship as in a plane submerged jet.

Zhestkov, Glazkov, and Gusev investigated the velocity and temperature fields occurring in the mixing zone of two plane-parallel turbulent jets moving in the same direction at different velocity and temperature ratios. The initial cross sections of each of the adjoining jets were rectangular in shape with sides 40×125 mm, the long side being common to both. The partition dividing the jets up to the point of contact was 2 mm thick. Figure 1.20 shows the velocity fields obtained during this investigation in the mixing zone at a distance $x=100$ mm from the beginning of mixing, at the following discharge velocity ratios: $m=u_{II}/u_0$ 0, 0.23, 0.43, and 0.64, and almost identical initial temperatures (the temperature of the jet at the higher velocity varied between $t_0=50$ and 53°C ; the temperature of the second jet was $t_{II}=27$ to 44°C).

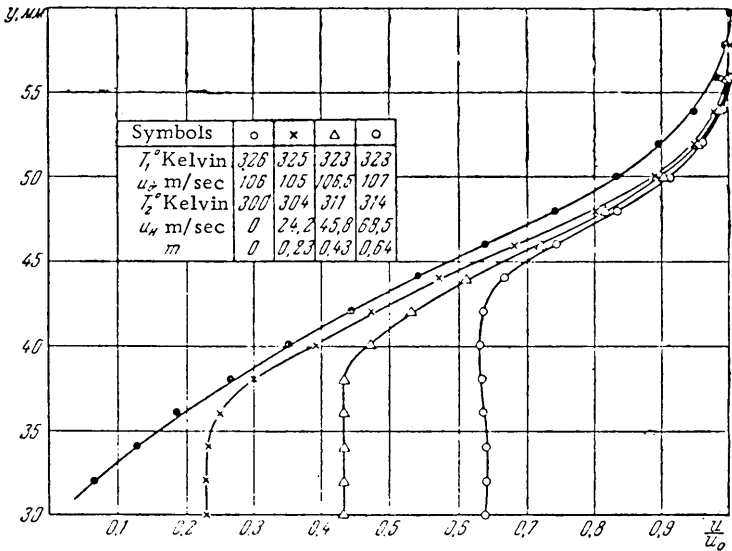


Fig. 1.20. Velocity profiles in boundary layer of two coflowing plane jets (initial region) according to Zhestkov et al.

The ratio of initial velocities was varied by altering the velocity of the second (slower) jet, while the velocity of the active jet hardly varied and was $u_0=105$ to 107 m/sec.

Figure 1.21 shows the same velocity fields in the following dimensionless coordinates: $\frac{\Delta u}{\Delta u_0} = f\left(\frac{\Delta y_c}{\Delta y_b}\right)$, in which $\Delta u = u - u_1$ is the surplus velocity in the jet; $\Delta u_0 = u_0 - u_{II}$ is the initial difference between the velocities in the jet; $\Delta y_c = y - y_c$ is the cross distance between the point of measurement and the point at which the velocity $\Delta u_c = 0.5 \Delta u_m$; $\Delta y_b = (y_{0.9} - y_{0.1})$ is the distance between the points at which the surplus velocities are, respectively, $\Delta u_1 = 0.9 \Delta u_0$

and $\Delta u_2 = 0.1 \Delta u_0$. This graph also plots the velocity curve taken from Figure 1.9 (broken line) obtained from the experiments of Albertson et al. It is not difficult to see that the dimensionless profile of the surplus velocity in the mixing zone of two plane-parallel jets having the same direction is universal and coincides with the profile in the boundary layer of a plane-parallel submerged jet.

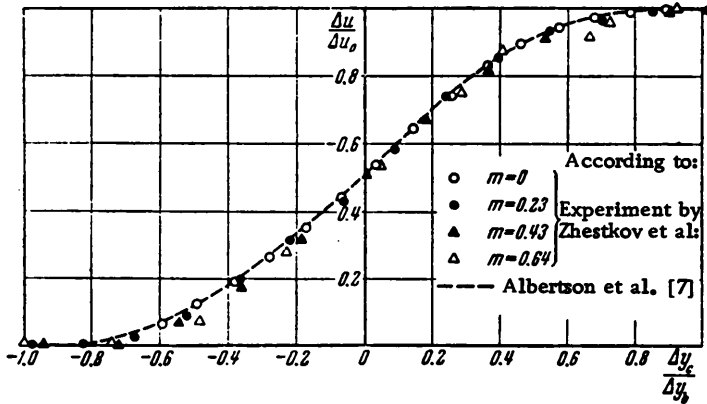


Fig. 1.21. Dimensionless velocity profiles in boundary layer of two plane coflowing jets of air (initial sector) according to the experimental data of Zhestkov, et al.

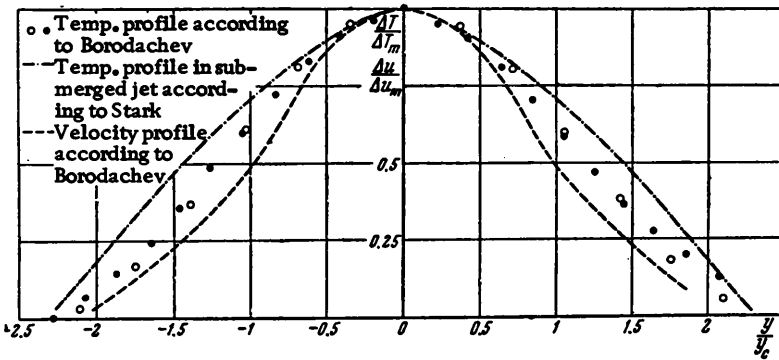


Fig. 1.22. Dimensionless temperature in main region of axially symmetric jet spreading through coflowing air stream according to Borodachev's experimental data.

Figure 1.22 shows a universal profile for the dimensionless temperature difference in the main region of an axially symmetric jet when there is a coflowing external air stream,

$$\frac{T - T_u}{T_m - T_u} = f\left(\frac{y}{y_c}\right),$$

obtained in Borodachev's experiments (dissertation) at a velocity ratio $m = u_n/u_0 = 0.185$ ($u_0 \approx 125$ m/sec), and a temperature difference in the initial section of the active jet $\Delta T_0 = 320^\circ$ and a temperature of the coflowing stream of about 20°C ; the temperature fields were determined at different distances from the nozzle (up to 40 diameters).

For purposes of comparison, Figure 1.22 shows an experimental temperature profile (dots and dashes) in a submerged jet, taken from Figure 1.16; furthermore, Figure 1.22 shows the velocity profile from Borodachev's experiments (broken line). Evidently, the dimensionless profile of the temperature difference depends scarcely at all on the presence of a coflowing stream of fluid, but differs from the velocity profile.

Figure 1.23 shows temperature differences obtained by Zhestkov and others for the plane-parallel mixing zone of two jets, described above, at the following ratios of initial velocity and corresponding initial temperatures

$$m = 0.3, \quad t_0 = 51^\circ\text{C}, \quad t_n = 32^\circ\text{C};$$

$$m = 0.5, \quad t_0 = 50^\circ\text{C}, \quad t_n = 38^\circ\text{C}.$$

The ordinate plots the ratios $\Delta T/\Delta T_0$, in which $\Delta T_0 = t_0 - t_n$, while the abscissa plots the same values of $\Delta y_c/\Delta y_b$ as in Figure 1.21. For purposes of comparison, Figure 1.23 shows the temperature curve (dotted line) taken from Figure 1.14 and referred to the boundary layer of the initial region of a submerged axially symmetric jet; furthermore, Figure 1.23 shows the dimensionless velocity curve (solid line) for a boundary layer taken from Figure 1.21.

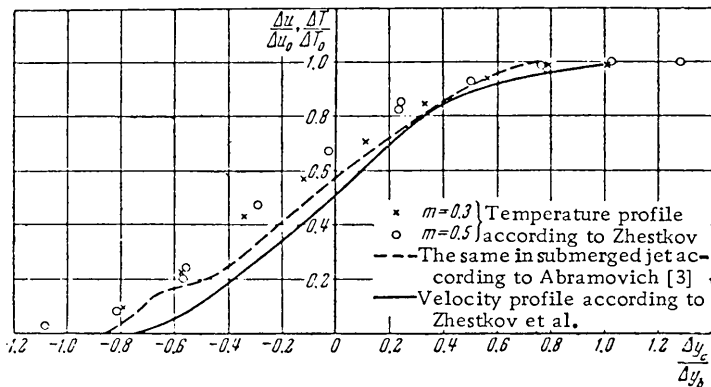


Fig. 1.23. Dimensionless profiles of temperature difference in boundary layer between two plane co-flowing jets of air (initial region) according to the data of Zhestkov et al.

It follows from Figure 1.23 that the dimensionless temperature field in the plane parallel boundary layer is universal and not a function of the velocity of the coflowing stream; furthermore, it does not coincide with the dimensionless velocity field.

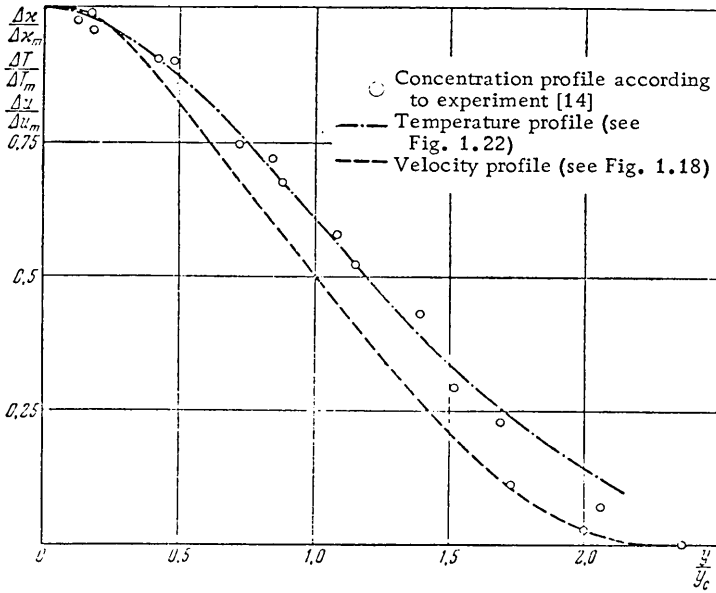


Fig. 1.24. Dimensionless profiles for concentration of admixture by weight (helium) in main region of axially symmetric air jet in coflowing stream of air according to Forstall and Shapiro [14].

Figure 1.24 shows a universal field of dimensionless values for helium concentration by weight, obtained in the main region of an axially symmetric air jet with an admixture of helium spreading through a coflowing stream of air ($x_n = 0; \Delta x = x$):

$$\frac{x}{x_m} = f\left(\frac{y}{y_c}\right).$$

The experiments carried out by Forstall and Shapiro [14] with the same experimental equipment on which were obtained the previously considered velocity fields were made at an external flow velocity $u_{\infty} = 0.5u_0$ and a nozzle diameter 12.7 mm. The initial helium concentration in the jet was $x_0 = 0.1$. Figure 1.24 shows the dimensionless temperature difference, taken from Figure 1.22, which almost coincides with the concentration profile.

The experimental data that we have given shows that when a turbulent jet spreads through a coflowing flow of fluid, the profiles for the admixture concentration in the cross sections of the jet are similar to the temperature profiles and dissimilar to the

velocity profiles; the presence of a coflowing stream has no effect on the nature of the velocity, temperature, or concentration distribution in the cross sections of the jet.

Let us now consider the experimental data available, which are regrettably very scant, on the velocity and temperature distribution in a jet interacting with a counterflowing stream of fluid, for example, in the initial region of flow beyond a poorly streamlined body, beyond the base of which there are reverse stream lines.

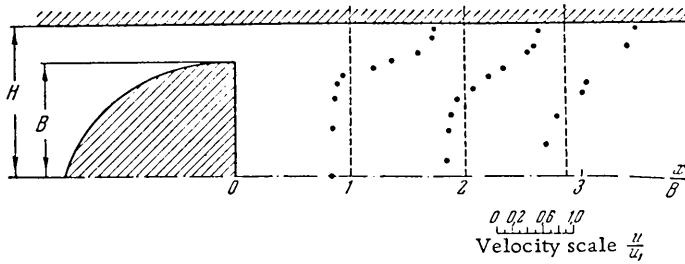


Fig. 1.25. Velocity profiles in wake behind plane blunt body according to experiments carried out by Abramovich and Vafin.

Figure 1.25 shows the dimensionless velocity profiles behind the base of a two-dimensional semistreamlined body situated symmetrically with respect to the axis of a plane channel of constant section:

$$\frac{u}{u_1} = f\left(\frac{y}{h}\right);$$

here y is the distance from the channel wall; $h = H - B$ is the initial thickness of the jet emerging from a slot formed by the wall of the channel and the surface of the body (H is the half-height of the channel, B is the half-thickness of the body); u is the local stream velocity; u_1 is the velocity in the initial section of the jet. Points have been taken from experiments carried out by the author in collaboration with F. M. Vafin; the points were obtained for channel sections located at different distances from the base of the body ($x/B = 1, 2$, and 2.88), at which the relative velocity of the reverse flow varied between $-u_2/u_1 = 0$ to 0.35 . Similar experiments were carried out at several ratios of the body thickness to channel height: $\xi = B/H = 0.4; 0.5; 0.6; 0.75; 0.83$. In width the body filled the whole channel.

Figure 1.26 shows these velocity profiles in the form

$$\frac{\Delta u}{\Delta u_0} = f\left(\frac{\Delta y_c}{\Delta y_b}\right),$$

in which $\Delta u_0 = u_1 - u_2$, and u_1 is the maximum velocity in the jet; u_2 is the minimum velocity of the back stream in the same section

($u_2 < 0$); Δy_c is the distance between the given point in the section and the point with velocity $\Delta u_c = 0.5 \Delta u_0$; Δy_b is the distance between the points with velocities $\Delta u = 0.9 \Delta u_0$ and $\Delta u = 0.1 \Delta u_0$. Figure 1.26 also shows the velocity distribution curve in the mixing zone of the initial sector of plane submerged jet (broken line), taken from the experiments of Albertson et al. (Fig. 1.9).

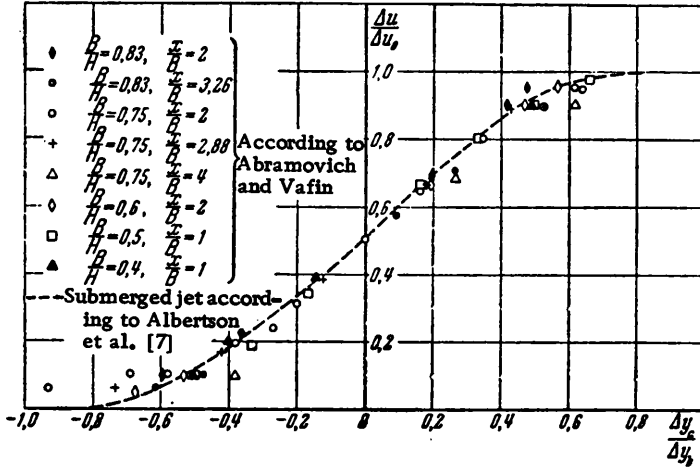


Fig. 1.26. Dimensionless surplus velocity profile behind plane poorly streamlined body according to Abramovich and Vafin.

The experimental data shown in Figure 1.26 indicates that the dimensionless velocity difference profiles in a plane jet bordering on a backstream of fluid are universal and are practically unchanged from those obtained for a submerged jet or those for a jet spreading into a coflowing stream (see Fig. 1.21).

Figure 1.27 shows the results of similar measurements made by the author in collaboration with F. M. Vafin in an axially symmetric channel with a body of circular section; measurements were made at different distances from the body ($x/B = 0.67; 1.33; 2.2$) at a relative body section area $\zeta = (B/R)^2 = 0.36$ (B is the radius of the body and R is the radius of the channel); the relative velocity of the backstream varied along the length between $-u_2/u_1 = 0$ to 0.4 . The dimensionless surplus velocities obtained in these experiments are shown in Figure 1.28 which also plots an averaged velocity curve (broken line) for the initial region of an axially symmetric jet, taken from Figure 1.7. Thus, the dimensionless velocity profile in the mixing zone proves to be universal and equally applicable to jets spreading through coflowing or counterflowing streams as well as to submerged jets.

Similar results are obtained for the combustion chamber of gas turbine engines. At the beginning of the chamber there is usually a large region of reverse flow adjoining the axis of symmetry.

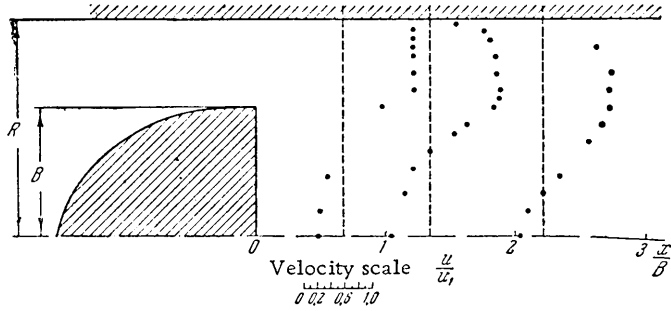


Fig. 1.27. Velocity profiles in wake behind axially symmetric poorly streamlined body according to Abramovich and Vafin.

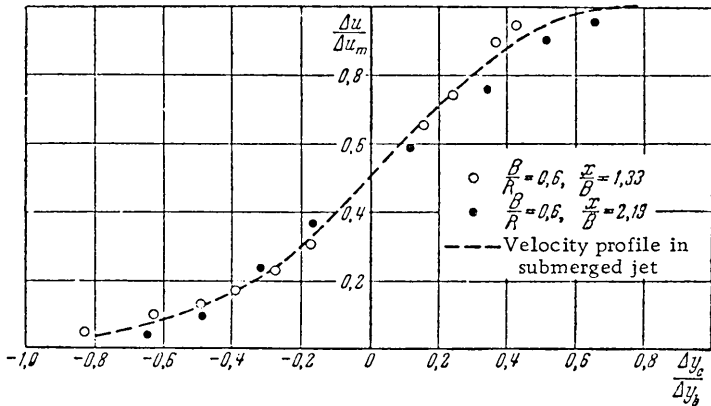


Fig. 1.28. Dimensionless surplus velocity profile in wake behind axially symmetric body according to Abramovich and Vafin.

Typical profiles for the axial components of velocity in different sections of a chamber, obtained during "cold blasting" (without combustion) by Mikhaylov [18] are shown in Figure 1.29. Figure 1.30 shows the same profiles, but in dimensionless coordinates (as in Figs. 1.26 and 1.28), and it also shows the corresponding averaged velocity curve (broken line) in the initial region of an axially symmetric submerged jet (Fig. 1.8). In this case as well, the dimensionless surplus velocity profile proved the same as for a submerged jet.

Figure 1.31 shows the flow pattern obtained by Vulis for the discharge of an air jet from a 20-mm nozzle into a counterflowing air stream emerging from a 100-mm nozzle; the velocity of the jet was $u_0 = 63$ m/sec, the velocity of the counterflowing stream u_H varied between 24 and 30 m/sec; in this manner it was possible to vary the velocity ratio over the range $m = 0.38$ to 0.47. Figure 1.31

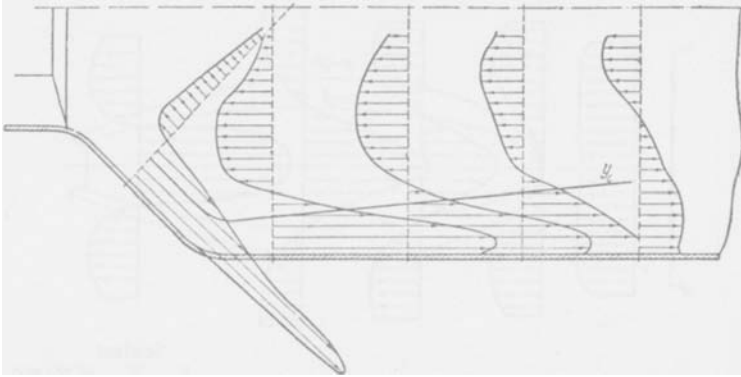


Fig. 1.29. Velocity profiles in combustion chamber of turbojet engine (with cold blast) according to Mikhaylov's data [18].

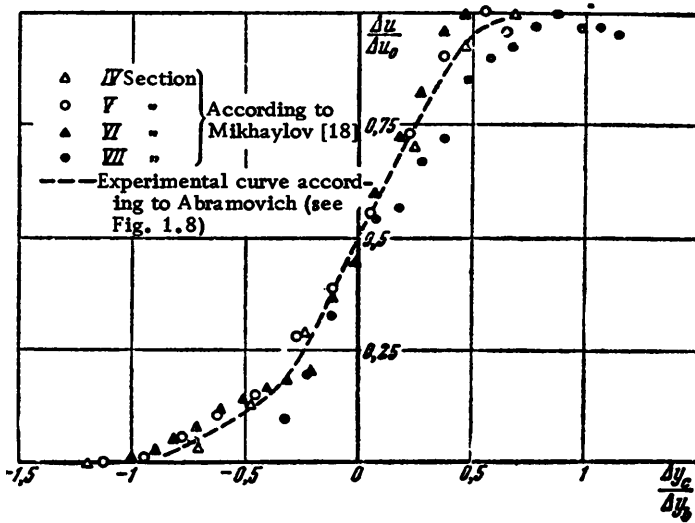


Fig. 1.30. Dimensionless surplus velocity profile in initial sections of turbojet engine combustion chamber according to Mikhaylov's data [18].

corresponds to a case in which $m=0.38$. Figure 1.32 plots data from Figure 1.31 for the dimensionless profiles of surplus velocity in the main region of the jet in the form

$$\frac{\Delta u}{\Delta u_0} = f\left(\frac{y}{y_c}\right),$$

in which $\Delta u = u - u_2$ is the surplus velocity in the jet; $\Delta u_0 = u_1 - u_2$ is the difference between the velocity on the jet axis and the velocity of the unperturbed counterflowing stream ($u_2 < 0$).

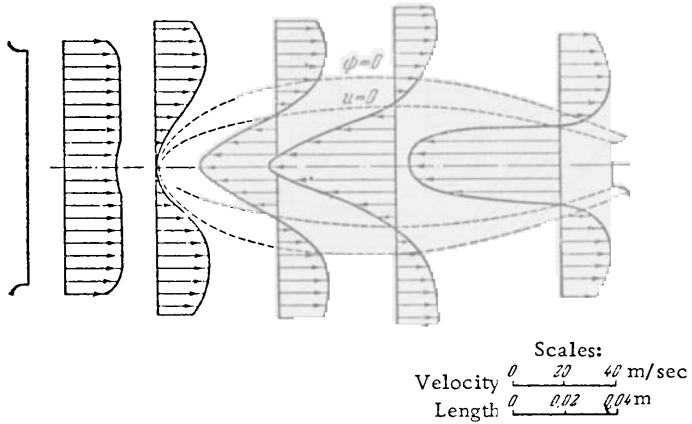


Fig. 1.31. Velocity profiles in different sections of an axially symmetric air jet in a counterflowing air stream according to Vulis's data [19].

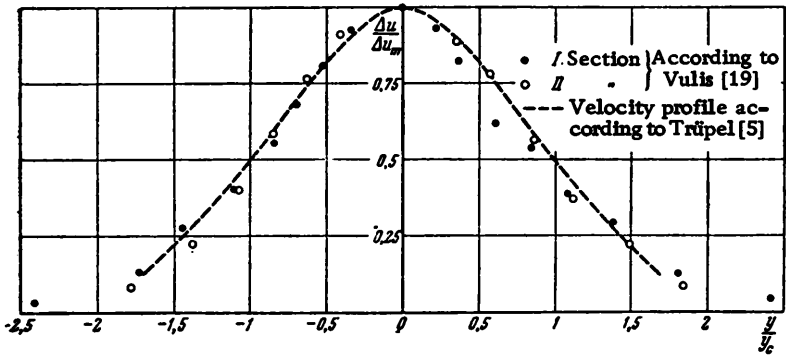


Fig. 1.32. Dimensionless surplus velocity profile in an axially symmetric jet in a counterflowing air stream according to Vulis [19].

The figure also shows an experimental profile (broken line) for a submerged jet, taken from Trüpel's data; the dimensionless profile for the surplus velocity in both cases is approximately the same.

1.10. Spread of a Turbulent Jet into a Coflowing or Counterflowing External Stream

The spread of a turbulent jet into a coflowing stream can be assessed in the same way as for a submerged jet in Section 1.4 [20, 21].

Let us assume that the rate of increase in the thickness of the boundary layer is proportional to the perturbation component of the transverse velocity

$$\frac{db}{dt} \sim v',$$

which, in its turn, is proportional to the transverse gradient of the longitudinal (principal) velocity of the flow

$$v' \sim l \frac{du}{dy},$$

in which l is the turbulent mixing length.

In view of the similarity of the velocity profiles in different sections of the boundary layer, the transverse gradient of the longitudinal velocity is proportional to the difference in velocities on the boundaries

$$\frac{du}{dy} \sim \frac{u_1 - u_2}{b},$$

on the basis of which,

$$v' \sim \frac{l}{b} (u_1 - u_2).$$

But it follows from this same condition (the similarity of the profiles) that the ratio between the characteristic linear dimensions is constant

$$\frac{l}{b} = \text{const.}$$

Thus, the perturbation component of the transverse velocity is proportional to the difference in velocities at the boundaries of the layer:

$$v' \sim u_1 - u_2$$

and, furthermore,

$$v' \sim \frac{db}{dt} = \frac{db}{dx} \frac{dx}{dt}$$

in which

$$\frac{dx}{dt} = u.$$

Hence, the law governing the increase in thickness of the boundary layer takes the following form:

$$\frac{db}{dx} \sim \frac{|v'|}{|u|} = \varepsilon \sim \frac{|u_1 - u_2|}{|u|}. \quad (1.35)$$

The quantity ε that is termed the degree of turbulence of the flow is scalar; it can be calculated from the mean absolute values of the transverse perturbation velocity $|v'|$ and the longitudinal velocity $|u|$ of the flow, because of which in all cases $\frac{db}{dx} > 0$. It

now remains to work out which value of the forward velocity should be substituted into the denominator in Eq. 1.35.

The mean characteristic velocity can be determined in different ways. It is the thickness (and not the cross sectional area) over which the velocity should be averaged; this is because of the above-established experimental fact that the increase in the thickness of plane and axially symmetric jets are approximately the same. For example, the mean mass velocity with respect to the thickness of a jet of variable density is

$$u = \frac{\int_1^2 \rho u dy}{\int_1^2 \rho dy} \quad (1.36)$$

For an incompressible fluid, this value is close to the arithmetic mean* of its absolute values on the boundaries of the layer

$$u = \frac{\int_1^2 u dy}{b} \approx 0,5 [|u_1| + |u_2|]. \quad (1.37)$$

In this case, we obtain the following law for the rate of growth of the thickness of the boundary layer

$$\frac{db}{dx} \sim \frac{|u_1 - u_2|}{|u_1| + |u_2|}. \quad (1.38)$$

Equation 1.38 leads to interesting conclusions. In the boundary layer occurring on the boundary between two infinite jets ($u_1 = \text{const}$, $u_2 = \text{const}$), the thickness is proportional to the distance from the beginning of mixing:

$$\frac{db}{dx} = \text{const}, \text{ or } b = \text{const} \cdot x,$$

*This result has been obtained by using the velocity profile and the cross section of the jet found in Chapter 2.

in which

$$\text{const} = c \frac{|u_1 - u_2|}{|u_1| + |u_2|}. \quad (1.39)$$

The constants in Eq. 1.39 can be determined from the results of the study of a jet spreading through a stationary medium ($u_2=0$) when the following equality holds

$$b_3 = cx. \quad (1.40)$$

In the general case ($u_2 \neq 0$), the thickness of the boundary layer is determined on the basis of Eqs. 1.38, 1.39, and 1.40:

$$\frac{b}{b_3} = \frac{|u_1 - u_2|}{|u_1| + |u_2|}. \quad (1.41)$$

In a particular case of two coflowing infinite jets, the velocities on the layer boundaries have the same sign; therefore,

$$\frac{b_n}{b_3} = \pm \frac{u_1 - u_2}{u_1 + u_2}, \quad (1.42)$$

the minus sign being taken when $u_2 < u_1$.

When a jet spreads through a counterflowing stream, the velocities on the layer boundaries have different signs, i.e., the geometric velocity difference is equal to the sum of the absolute velocities; hence,

$$\frac{b_n}{b_3} = \frac{u_1 + u_2}{u_1 + u_2} = 1. \quad (1.43)$$

In other words, during counterflowing motion of the jets ($u_2 < 0$), the angle of thickening of the boundary layer is not a function of the ratio of the velocities on the boundaries; that is, in all cases it is the same as for a jet spreading through a stationary medium; during coflowing motion of jets ($u_2 > 0$), the angle of thickening of the boundary layer decreases as the velocity of the coflowing stream increases:

$$\frac{b_\partial}{b_3} = \frac{1-m}{1+m}, \text{ where } m = \frac{u_2}{u_1}. \quad (1.44)$$

Equation 1.44 is valid only at $m < 1$. Indeed, as has been pointed out earlier, the thickness of the mixing zone is a positive value and is determined by the absolute velocity difference on its boundaries, irrespective of the sign that this difference may have. Thus, in the general case of coflowing motion of two jets, the

following expression, derived from Eq. 1.37 and also 1.39 and 1.44, holds:

$$\frac{db}{dx} = \pm c \frac{u_1 - u_2}{u_1 + u_2}. \quad (1.45)$$

Here, the plus sign is taken at $u_1 > u_2$, and the minus sign at $u_1 < u_2$. If both jets are infinite ($u_1 = \text{const}$, $u_2 = \text{const}$), then we find from Eq. 1.45 that

$$\frac{b}{x} = \pm c \frac{1 - m}{1 + m}. \quad (1.46)$$

As has already been pointed out, during counterflow of the jets, the thickness of the mixing zone is not a function of the velocity ratio on the boundaries; that is, it remains the same as for a submerged jet:

$$(1.47)$$

The constant c in Eqs. 1.45 to 1.47 is determined experimentally.

Figure 1.33 shows shadow photographs of the boundary layer occurring on the boundary between two plane jets of air at temperatures $T_{II} = 318^\circ\text{K}$ and $T_0 = 462^\circ\text{K}$, obtained by Zhestkov and others.

The velocity of the heated jet amounted to about 100 m/sec, while the velocity of the cold jet ranged from 0 to about 60 m/sec; the corresponding velocity ratios m for each photograph are shown in Figure 1.33.

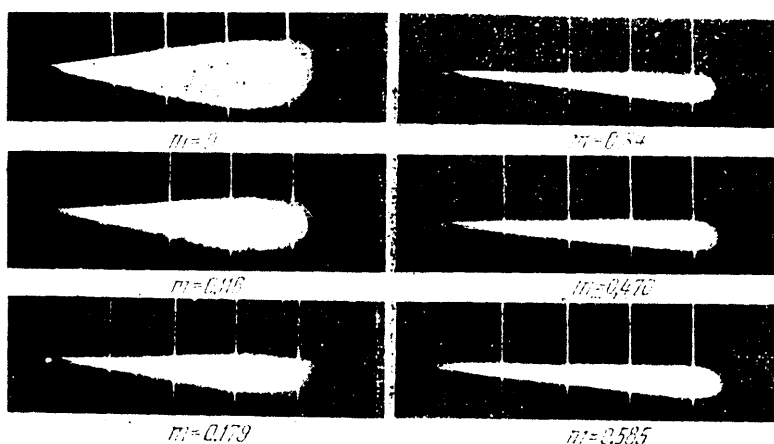


Fig. 1.33. Shadow photographs of a boundary layer between two coflowing plane jets.

We can see that during the increase in m from 0 to 0.34 the thickness of the boundary layer, which is clearly visible in the photographs, drops appreciably, and remains almost unchanged as m is further increased.

Figure 1.34 shows a theoretical curve for Eqs. 1.43 and 1.44 for a range of m from -1 to 0 and from 0 to $+1$:

$$\frac{\frac{1}{c} \frac{db}{dx}}{\frac{1}{c_3} \frac{db_3}{dx}} = 1 \quad \text{for } m \leq 0$$

and

$$\frac{\frac{1}{c} \frac{db}{dx}}{\frac{1}{c_3} \frac{db_3}{dx}} = \frac{1-m}{1+m} \quad \text{for } m \geq 0,$$

In view of the difficulty of determining the true thickness of the jet boundary layer b by experiment, here, as in Section 1.9, we use the distance Δy_b between the points with surplus velocities $\Delta u_1 = 0.9 \Delta u_0$ and $\Delta u_1 = 0.1 \Delta u_0$; for a universal velocity profile, Δy_b comprises the same proportion of the boundary layer thickness in all cases

$$\frac{\Delta y_b}{\Delta y_{b_3}} = \frac{b}{b_3},$$

in which b_3 is the boundary layer thickness of a submerged jet and Δy_{b_3} is the value Δy_b for a submerged jet.

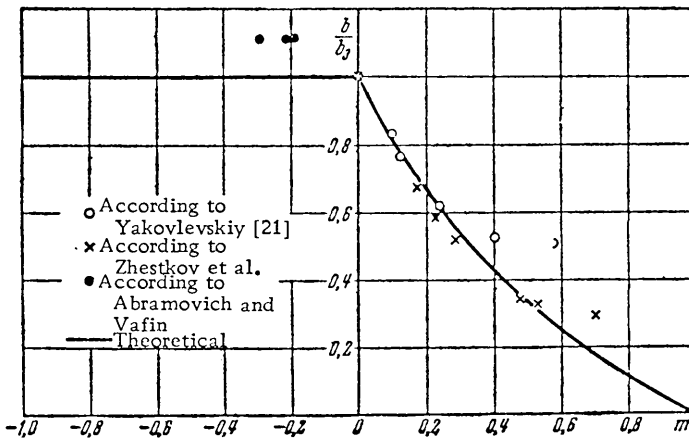


Fig. 1.34. Thickness of boundary layer of incompressible fluid jet as function of outside stream velocity.

The experimental points plotted on Figure 1.34 have been borrowed from the experiments carried out by Zhestkov and others, described in Section 1.9, and Yakovlevskiy [21] and others.

All the experimental points are close to the theoretical curve in the region $-0.4 < m < 0.4$ at the same experimental constant ($c = c_3$) but differ from it at $m > 0.5$. This result, likewise detectable in the photographs in Figure 1.33, can be explained in the following way. When deriving Eq. 1.44, we assumed that the turbulence in the boundary layer was caused only by the velocity difference on its boundaries, and that beyond these boundaries it did not exist at all, i.e., we assumed that as $m \rightarrow 1$, $v' \rightarrow 0$. But in actual fact there is a certain initial turbulence in an unperturbed stream as well. Hence, in cases in which the velocities u_1 and u_2 are close to each other, i.e., when the intensity of the turbulence in the jet is less than that of the unperturbed stream, the influence of the jet ceases and the growth is determined by the turbulence of the unperturbed stream which is not a function of m ; it is natural that in this regime the angle of thickening of the boundary layer is hardly associated with the velocity ratios of the layer boundaries.

The results obtained for the mixing zone for two infinite jets also relate to the initial region of a jet of finite thickness spreading through a coflowing or counterflowing stream, since in the initial region the velocities remain unchanged on both boundaries of the mixing zone.

The outer edge of the main region of a jet of finite thickness with counterflow of the fluid surrounding the jet remains the same as in a submerged jet, because the velocity of the counterflow has no effect on the angle of thickening of the mixing zone.

It is a more complex task to determine the outline of the main region of the jet in a coflowing fluid.

In this case Eq. 1.45 acquires the following form:

$$\frac{db}{dx} = \pm c \frac{u_m - u_n}{u_m + u_n}, \quad (1.48)$$

in which u_m is the velocity on the axis of the main region of the jet, u_n is the velocity of the coflowing stream (the minus sign is taken when $u_n > u_m$). Since u_m varies on the jet axis, i.e., $u_m = f(x)$, the jet boundary in a coflowing stream must be curved:

$$\frac{db}{dx} = \text{var.} \quad (1.49)$$

In order to determine the jet boundary, the form of the function $u_m(x)$ must be known, and can be obtained from the condition of conservation of momentum in the same way as was done in Section 1.6 for a submerged jet. The solution of this problem will be given in Chapter 5, which deals with the theory of a turbulent jet in a coflowing fluid.

1.11. Turbulence Characteristics in a Free Jet

In the theory of turbulence in general, and in the theory of a turbulent jet in particular, the laws governing the distribution of different pulsation characteristics of the stream and their interrelationships are very important. The perturbations of the velocity vector (or one of its components), averaged with respect to time, is equal to zero; hence it is usual to determine the turbulence of the flow from the nondisappearing mean-square pulsations in

velocity, temperature and other parameters $\sqrt{\overline{u'^2}}$, $\sqrt{\overline{v'^2}}$, $\sqrt{\overline{t'^2}}$, and so forth.

The interrelationship between the turbulent characteristics is determined by the mean values of their products (correlation) $\overline{u'v'}$, $\overline{u't'}$, $\overline{v't'}$, and so on. The averaged mixing length, which in accordance with Section 1.4, can be determined in the following way, serves as the measure of the scale of turbulence:

$$l_u = \frac{\sqrt{\overline{u'^2}}}{\frac{\partial \bar{u}}{\partial y}}, \quad l_v = \frac{\sqrt{\overline{v'^2}}}{\frac{\partial \bar{u}}{\partial y}}, \quad l_t = \frac{\sqrt{\overline{t'^2}}}{\frac{\partial \bar{t}}{\partial y}}.$$

Below we give the results, obtained by Antonova, of an experimental study of turbulence characteristics for a free heated turbulent jet.

In the experiments the mean velocity fields in the sections of the jet were determined, and the velocities were measured both with a T-shaped probe and also a hot wire. The pulsation velocities of the stream and the mean and pulsation temperatures were measured with a hot wire having a single-filament tungsten probe with a filament diameter of 20 microns, and a ETA-1A device developed by P. V. Chebyshev. The measurements were taken under the following conditions and in the following sections of the jet:

| Condition | Jet parameters upon leaving nozzle | | | Main region $\frac{x}{d}$ | Initial region $\frac{x}{d}$ |
|-----------|------------------------------------|-------------------|-------------------------|---------------------------|------------------------------|
| | u_0 m/sec | $t^\circ\text{C}$ | $R = \frac{u_0 d}{\nu}$ | | |
| I | 35 | 225 | $39.3 \cdot 10^3$ | 7.5 | 0.25 |
| II | 35 | 100 | $59 \cdot 10^3$ | 8.75 | 2.25 |
| III | 30 | 125 | $30.5 \cdot 10^3$ | 10 | 4.25 |

The results of the measurements of the mean velocities and temperature differences in various cross sections of the jet are shown in dimensionless coordinates in Figure 1.35a, b, and c. Here, the local velocities and temperature differences, respectively,

are referred to the velocity and temperature difference on the axis of each section:

$$\frac{u}{u_m} = f\left(\frac{y}{b}\right), \quad \frac{\Delta T}{\Delta T_m} = f\left(\frac{y}{b}\right),$$

in which y is the distance between the jet axis and the point investigated in the main region, and the distance between the nozzle edge and the point investigated in the initial region; b , b_1 is the half-thickness (radius) of the jet at the given cross section of the main region or the half-thickness of the boundary layer in the initial region. These graphs also show the gradients of velocity and temperature.

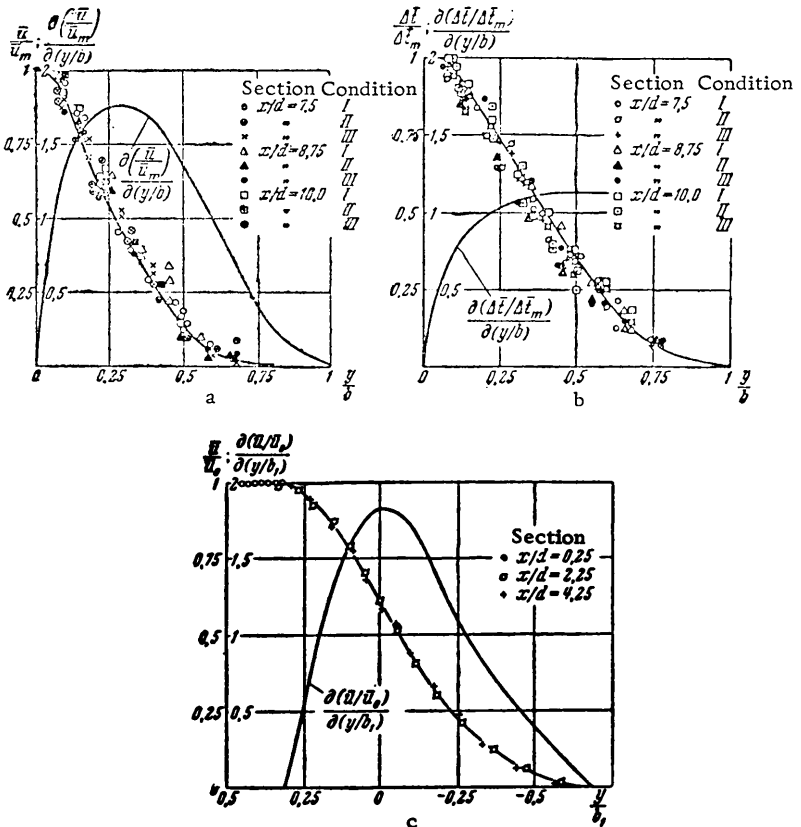


Fig. 1.35. Fields of mean velocity, gradient of mean velocity, mean temperature, and gradient of mean temperature in jet (a and b are in main region, and c in initial region).

The results of measuring the turbulence characteristics are shown in Figure 1.36 in the following dimensionless form:

$$\frac{\sqrt{\overline{u'^2}}}{\bar{u}_m}, \quad \frac{\sqrt{\overline{v'^2}}}{\bar{u}_m}, \quad \frac{\sqrt{\overline{t'^2}}}{\Delta T_m} \quad K_{uv}, \quad K_{vt}, \quad K_{ut},$$

as functions of the dimensionless ratio $\frac{y}{b}$. Here, $\sqrt{\overline{u'^2}}, \sqrt{\overline{v'^2}}, \sqrt{\overline{t'^2}}$ are the mean-square perturbations of the longitudinal and transverse components of the velocity vector and of the temperature, while

$$K_{uv} = \frac{\overline{u'v'}}{\sqrt{\overline{u'^2}} \sqrt{\overline{v'^2}}}, \quad K_{vt} = \frac{\overline{v't'}}{\sqrt{\overline{v'^2}} \sqrt{\overline{t'^2}}}, \quad K_{ut} = \frac{\overline{u't'}}{\sqrt{\overline{u'^2}} \sqrt{\overline{t'^2}}}$$

are the correlation coefficients between the corresponding turbulent pulsations.

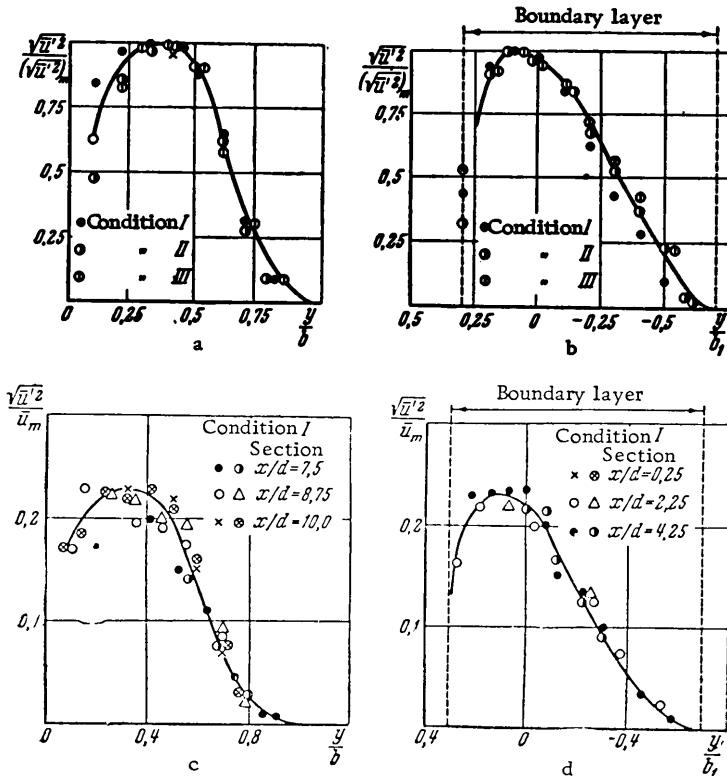


Fig. 1.36. Pulsation fields for longitudinal velocity component in sections of nonisothermal jet (a and c in the main region, b and d in the initial region).

The measurements show that the mean-square pulsations of the longitudinal component of the velocity vector in the cross sections of the main region of the jet can be represented with a fair degree of accuracy by the curve shown in Figure 1.36a and b. Since the range over which the Reynolds numbers were varied is fairly narrow, no conclusions with regard to the similarity of the mean-square pulsations of the longitudinal component of the velocity vector can be drawn on the basis of these experiments.

If it is assumed that the following equality holds:

$$\sqrt{\overline{u'^2}} = l_u \frac{\partial \bar{u}}{\partial y}, \quad (1.50)$$

then we can find the value of l_u , known as the mixing length. The mean velocity gradient with respect to thickness of the section in the main region of the jet is shown in Figure 1.35a. The dimensionless quantity l_u/b , found from the given experiments and from Eq. 1.50, remains roughly constant for most of the cross section and is 0.12 to 0.13.

In the initial region of the jet, the distribution of the pulsation of the longitudinal component of the velocity vector, shown in dimensionless coordinates

$$\frac{\sqrt{\overline{u'^2}}}{\bar{u}_0} = f\left(\frac{y}{b_1}\right),$$

can also be described reasonably accurately by a single curve (see Fig. 1.36 b and d). The assumption of the validity of Eq. 1.50 in the boundary layer of the initial region made it possible to determine l_u/b_1 , which proved to be approximately 0.1 for most of the cross section of the boundary layer.

The mean-square pulsations in the transverse component of the velocity vector in the sections of the main region are shown in

dimensionless coordinates $\sqrt{\overline{v'^2}}/\bar{u}_m$ and y/b in Figure 1.37 a and c; they can also be described reasonably accurately by a single curve (Fig. 1.37a and c) over the range of Reynolds numbers under investigation. Assuming the validity of the relation

$$\sqrt{\overline{v'^2}} = l_v \frac{\partial \bar{u}}{\partial y},$$

we can also find the mixing length l_v . The ratio l_v/b is more or less constant for most of the section, and is equal to 0.1. The mean-square pulsations in the transverse component of the velocity vector in the boundary layer of the initial region are shown in

dimensionless coordinates $\sqrt{\overline{v'^2}}/\bar{u}_0$ and y/b_1 in Figure 1.37b and d. The mixing length of the transverse velocity vector component in

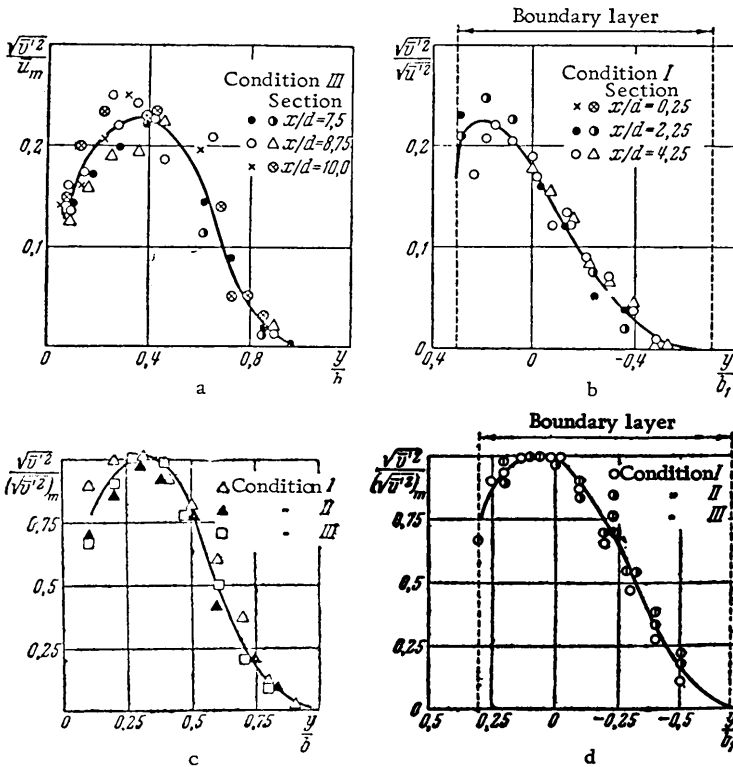


Fig. 1.37. Fields for pulsation of transverse velocity component in sections of nonisothermal jet (a and c are in the principal region; b and d in the initial region).

the boundary layer of the initial region is approximately equal to $0.08 b_1$. The distribution of pulsations in the longitudinal and transverse velocity vector components are close together and identical in nature.

The mean-square pulsations in temperature in the sections of the main region of a free heated jet are plotted in Figure 1.38a and b in dimensionless coordinates. The considerable spread of the experimental points in Figure 1.38 suggests that there is no universal curve for the temperature pulsation profile in different cross sections of the jet.

The correlation coefficients for the pulsations in the longitudinal component of velocity and the temperature, measured in cross sections of the jet, are shown in Fig. 1.39. Similar experiments for determining the turbulence characteristics in the main region of a free nonisothermal jet are described in References [39 and 55]. The dimensionless pulsations given in these publications coincide with those described above, except for the correlation coefficient between the pulsations in the longitudinal component

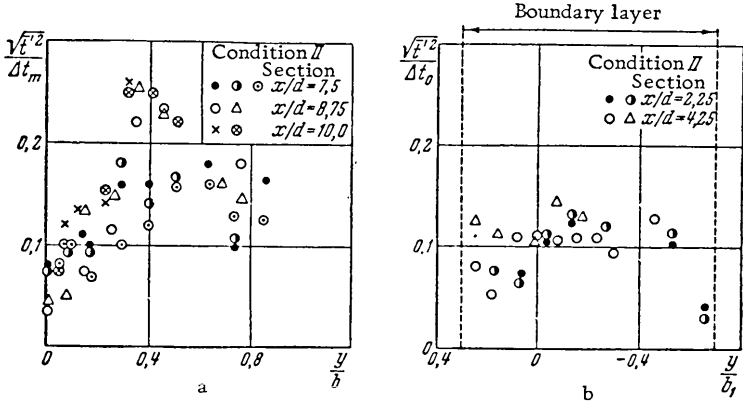


Fig. 1.38. Temperature pulsation fields in sections of nonisothermal jet (a is principal region, b is initial region).

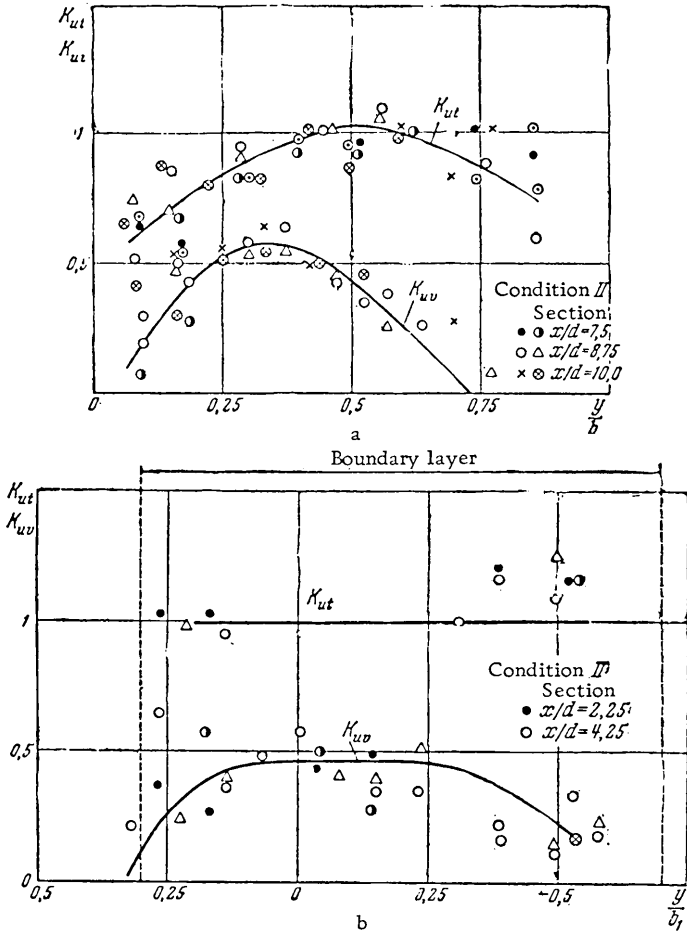


Fig. 1.39. Variation in correlation coefficients K_{uv} , K_{ut} in sections of nonisothermal jet (a—principal region, b—initial region).

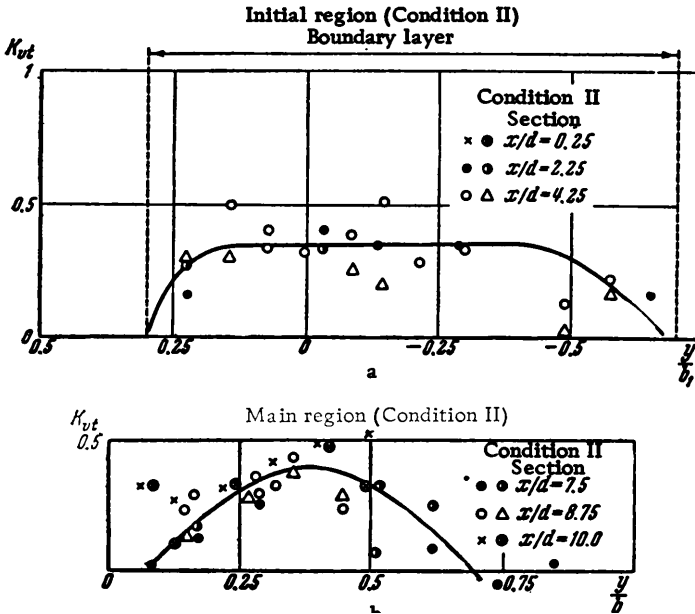


Fig. 1.40. Variation in correlation coefficient K_{vt} in sections of nonisothermal jet (a - principal region, b - initial region).

of velocity and the temperature K_{ut} . In Antonova's investigation (at $x/d = 7.5$ to 10) K_{ut} ranges between 0.6 and 1 ; in [39] ($x/d = 15$ to 20), it varies between 0.3 and 0.4 ; and in [55] ($x/d = 150$ to 300), it ranges from 0.3 to 0.6 and attains approximately 0.9 in some sections. The difference in K_{ut} arises from the difference in the methods used. In [39 and 55] it was actually the correlation coefficient between the pulsations in the velocity vector and the pulsations in temperature K_{wt} that was measured, rather than K_{ut} , as in Antonova's work.

The correlation coefficients K_{uv} , K_{ut} , and K_{vt} (Figs. 1.39 and 1.40) are expressed by universal curves; i.e., at corresponding points in any two sections the correlation coefficients are correspondingly identical. Furthermore, within the range of Reynolds numbers investigated, the correlation coefficients K_{uv} , K_{vt} , and K_{ut} do not vary in magnitude within the main and initial regions of the jet, respectively.